Applied Energy 211 (2018) 200–217

Contents lists available at ScienceDirect

Applied Energy

journal homepage: www.elsevier.com/locate/apenergy

Vanadium dioxide for energy conservation and energy storage applications: Synthesis and performance improvement

Shancheng Wang[a], Kwadwo Asare Owusu[c], Liqiang Mai[c,*], Yujie Ke[a], Yang Zhou[a], Peng Hu[a], Shlomo Magdassi[d], Yi Long[a,b,*]

[a] School of Materials Science and Engineering, Nanyang Technological University, 50 Nanyang Avenue, 639798, Singapore
[b] Singapore-HUJ Alliance for Research and Enterprise (SHARE), Nanomaterials for Energy and Energy-Water Nexus (NEW), Campus for Research Excellence and Technological Enterprise (CREATE), 138602, Singapore
[c] State Key Laboratory of Advanced Technology for Materials Synthesis and Processing, Wuhan University of Technology, Wuhan 430070, China
[d] Institute of Chemistry, Edmund Safra Campus, The Hebrew University, Jerusalem 91904, Israel

HIGHLIGHTS

- Elaborated six chemical vapor deposition (CVD) methods to growth VO_2 pure phase.
- Discussed the optimum conditions for VO_2 pure phase growth for various CVD methods.
- Strategies to improve VO_2's thermochromic and electrochemical performance.
- Future perspective to stimulate the research in energy saving and storage field.

ARTICLE INFO

Keywords:
Vanadium dioxide
Chemical vapor deposition
Atomic layer deposition
Smart-window
Lithium-ion battery
Supercapacitor

ABSTRACT

Vanadium dioxide (VO_2) is one of the most widely studied inorganic phase change material for energy storage and energy conservation applications. Monoclinic VO_2 [VO_2(M)] changes from semiconducting phase to metallic rutile phase at near room temperature and the resultant abrupt suppressed infrared transmittance at high temperature makes it a potential candidate for thermochromic smart window application to cut the air-condition usage. Meanwhile proper electrical potential, stable structure and good interaction with lithium ions make metastable VO_2 [VO_2(B)] an attractive material for fabrication of electrodes for batteries and supercapacitors. However, some long-standing issues have plagued its usage. In thermochromic application, high transition temperature (τ_c), low luminous transmittance (T_{lum}) and undesirable solar modulation ability ($\triangle T_{sol}$) are the key problems, while in energy storage applications, short cycling lifetime and complex three-dimension microstructure are the major challenges. The common methods to produce VO_2 polymorph are physical vapour deposition (PVD), chemical vapour deposition (CVD), sol-gel synthesis, and hydrothermal method. CVD is an intensively studied method due to its ability to produce uniform films with precise stoichiometry, phase and morphology control. This paper reviews the various CVD techniques to produce VO_2 with controlled phases and the ternary diagram shows the relationship between film stoichiometry and various process conditions. The difference between the various CVD systems are commented and the process window to produce VO_2 are tabulated. Some strategies to improve VO_2's performance in both energy conservation and energy storage applications are discussed.

1. Introduction

As the world population increasing, the energy demand of society increases rapidly. The world energy consumption in 2020 will increase to 53 billion kWh [1,2]. Because of the limited amount of conventional energy sources such as coal, crude oil and natural gas, the current energy consumption practice has been proved as unsustainable. To fulfil the requirement of sustainability, approaches such as cutting off energy usage and exploring cleaner energy source have to be employed.

Energy saving in building is one of the important tasks in energy usage cutting off since building is one of the largest energy usage sectors. According to the report from United Nations, human-made

* Corresponding authors.
E-mail addresses: mlq518@whut.edu.cn (L. Mai), longyi@ntu.edu.sg (Y. Long).

https://doi.org/10.1016/j.apenergy.2017.11.039
Received 10 July 2017; Received in revised form 30 October 2017; Accepted 5 November 2017

Nomenclature

AACVD	aerosol assisted chemical vapour deposition
ALD	atomic layer deposition
APCVD	atmospheric pressure chemical vapour deposition
AR-layer	anti-reflecting layer
CVD	chemical vapour deposition
CNT	carbon nanotube
DLI-MOCVD	direct liquid injection metal-organic chemical vapour deposition
FESEM	field emission scanning electron microscope
ITO	indium tin oxide
HVAC	heating, ventilation and air conditioning
MFC	mass flow controller
MIT	metal insulator transition
MOCVD	metal-organic chemical vapour deposition
PECVD	plasma enhanced chemical vapour deposition
PVD	physical vapour deposition
SEM	scanning electron microscope
SPR	surface plasmon resonance
τ_c	transition temperature
TEM	transmission electron microscope
TEMAV	tetrakis[ethylmethylamido]vanadium
T_{lum}	luminous transmittance
VLS	vapour-liquid-solid
$\triangle T_{sol}$	solar modulation ability

building consumes 40% of total primary energy requirement globally and emits 30% of annual carbon dioxide emission [3]. Within the energy usage in building, heating, ventilation and air conditioning (HVAC) applications use about 50% of total energy [4]. Based on these data, reducing energy consumption for HVAC becomes an important task for architect and engineer. The HVAC energy consumption can be reduced via both aggressive and passive ways such as improving the efficiency of air conditioning system, adding thermal insulating to the wall, using cooling roof, and installing smart window glazing [5–7]. Since the window is the most energy inefficient component in the building, regulation the heat through the window becomes an important consideration for designer and national standard [8,9]. Vanadium oxide (VO_2) is one of the phase change materials used as thermochromic smart window coating to cut off the energy consumption for regulating room temperature due to its near room temperature metal-insulator transition (MIT) and has attracted attention from academia and industry. When temperature increases above the transition temperature (τ_c), the material transits from insulator to metal and its lattice changes from monoclinic to rutile with a diminished transmittance in the near-infrared range [10]. Therefore, temperature dependent solar modulation can be triggered automatically. Based on the heat reflection and absorption effect from the metallic state of VO_2, the building in warm-area (Cairo, Palermo and Rome) that employs VO_2 coated smart window shows an annual energy saving up to 10% [11]. Although VO_2(M) is attractive as an energy conservation material, some limitations restrict its application: First, bulk VO_2(M) has a τ_c at ~68 °C, which is too high for room-temperature applications. Secondly, the integrated luminous transmission (T_{lum}) for VO_2(M) is only ~40% with a noticeable magnitude of solar modulation (ΔT_{sol}) < 20% which is insufficient for windows coating applications [12]. Nanothermochromism [13–15], controlled porous films [16], moth-eyed nanostructure [17], multi-layered antireflective over-coated films [18] and gridded structures [19–21] as shown in Fig. 1 have been investigated to address those issues. The organic [22] and hybrid structure [23,24] show superior T_{lum} and ΔT_{sol}, however they suffer from low durability and the translucent state at a high temperature, which is not favourable for window applications. In inorganic VO_2, the performance varies significantly due to the difficulty to control the crystallinity [25], uniformity, morphology [26] and phases because of its rich valence [27,28].

On the other hand, although the cleaner energy such as solar energy and wind energy have been successfully commercialised, it is still very far from fully replacing the fossil fuel because of several limitations of the cleaner energy. For example, the photovoltaic panel can only generate electrical power during the daytime, and the amount of electricity generated by wind turbine is not stable since the speed of wind changes with time. Those issues prevent the large-scale application of solar and wind energy in everyday life [29]. Moreover, the development of electric vehicles based on the requirement to get rid of fossil fuel raises higher demand to the large capacity energy storage device [30]. Meanwhile, energy storage technology is also used to harvest the wasted kinetic energy from vehicle and large machine [31,32]. Under this circumstance, metastable VO_2 [VO_2(B)] attracts attention in the energy storage area as battery and supercapacitor electrode materials and supercapacitor materials. VO_2(B) presents the advantage of having a proper electrode potential, which is desirable for batteries and supercapacitors [33]. Moreover, the unique tunnel structure of VO_2(B) allows lithium ion intercalate and deintercalate in reversible Li-ion battery [34]. Meanwhile, VO_2(B) has the outstanding resistance to the lattice shearing during charging cycling because of its increased edge shearing [35]. Lastly yet importantly, compared with the current cathode material in lithium battery such as $LiCoO_2$, the vanadium based cathode has lower cost due to the abundance in nature [36]. Since the morphology of electrode component has a significant influence on electrochemistry performance [37], a batch of one-dimension (1D) and two-dimensions (2D) structure such as nanorod [38], nanowire [39], nanobelt [40] and nanoparticles [41] have been produced. However, those structures suffer from poor cycling stability [42]. Three-dimensional (3D) microstructures such as flower-like structure [43], nanothorn hollow microsphere [42] and urchin-like structure [44] have been reported to exhibit superior cycling stability over 1D and 2D nanostructures because of the porous and rigid 3D structures. Meanwhile, several groups [45,46] proved that carbon coating on electrode effectively improved electrode cycling stability. Despite the advances of these two ideas, there are still have some limitations. First, the thick carbon coating is not preferred in supercapacitor and battery electrodes as it hinders the diffusion kinetics of Li-ion and slows down the charge/discharge rate [47], which eliminates the advantage of tunnel structure in VO_2(B) crystal, Second, the current commonly used method such as hydrothermal process is not good at controlling film thickness precisely.

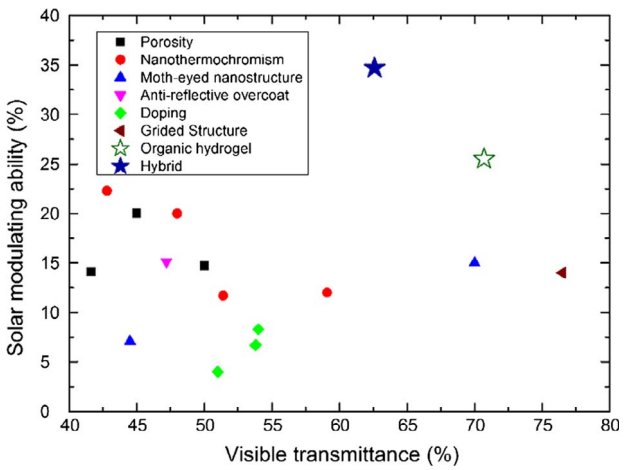

Fig. 1. Thermochromic performance of film produced by the various methods. Adapted from Ref. [24] with permission from Wiley.

Third, the complexity of the synthesis process for 3D microstructures and the difficulty in controlling the structure, stoichiometry and morphology also remain daunting tasks. Finally, current synthesis method is not suitable for large quantity production.

Compared with other fabrication methods such as physical vapour deposition (PVD) [48], sol-gel synthesis [13,18,21,49], polymer-assisted deposition [50,51], hydrothermal [52–54] and dip coating [55], CVD takes the advantages in producing high uniformity film with precise stoichiometric control on a large area. For example, a wafer-sized electronic-grade single crystalline VO_2 thin film fabricated with CVD has recently been produced by Zhang et al. [56]. Although the authors did not achieve mass production of VO_2, this case proved the capability of CVD to become an industrialised production technique. The objectives of this article are to review various CVD techniques used to deposit VO_2 thin film with controlled phases, to elaborate the processing parameters that affect the thin film quality and to discuss the strategies such as doping, forming of composite, ultra-thin overcoating and so forth (Fig. 2), which can improve the performance of the films. The different phases, lattice, space group of VO_2 and their applications are shown in Table 1.

2. Chemical vapour deposition (CVD) of VO_2

CVD is a thin film deposition technique that is widely used in semiconductor and other industries. It utilises precursor vapour or gas precursor to react in a reaction chamber and deposits the product of reaction onto a substrate to form a thin film. The scheme of the entire process is presented in Fig. 3. The precursors are first brought into the reaction chamber by the carrier gas (step 1) followed by the diffusion of the precursor from the main stream to the substrate, forming a boundary layer on the substrate surface (step 2a). In boundary layer, gas flow rate gradually decreases from main stream velocity to zero and the precursor is subsequently absorbed onto the substrate. Heterogeneous nucleation and reaction happen (step 3) with the film subsequently forming on substrates and coalescence (step 4). In contrast, in step 2b, homogeneous reaction may happen with powders produced above boundary layer and in most cases the film deposited with powders as crystallisation nuclei is not preferred due to poor adhesion and quality [61]. The by-products and unreacted precursor are transported out from the chamber at the end of the process (step 5a, 5b).

Depending on system configuration, there are several types of CVD system such as atmospheric pressure CVD (APCVD), plasma enhanced CVD (PECVD), metal-organic CVD (MOCVD) and so forth. These techniques to deposit VO_2 will be introduced in details later. The pros and cons of different CVD systems are summarised in Table 2.

2.1. Atmospheric pressure chemical vapour deposition (APCVD)

APCVD is the CVD technique with atmospheric chamber pressure. The technique utilises inert gas such as argon or nitrogen to fill the chamber and maintain chamber pressure. A typical APCVD system configuration is shown in Fig. 4, mass flow controller (MFC) is used to precisely control the flow rate of carrier gas. APCVD has a significant limitation: in order to produce sufficient precursor vapour, only volatile precursor can be used. The limitation restricts choosing of precursor, and sometimes bubbler has to be heated to ensure continuous vaporisation or sublimation of precursor.

Due to its simple system configuration, APCVD was applied to deposit VO_2 thin film from 1968 [64]. In that experiment vanadium(V) oxytrichloride ($VOCl_3$) and carbon dioxide (CO_2)/carbon monoxide (CO) mixture gas were used as precursors. The transition temperature for deposited VO_2 film was 67 °C, which was similar to τ_c of bulk VO_2. There are two types of precursors namely vanadium halide and vanadium-organometallic. In the vanadium halide system, two major precursors VCl_4 and $VOCl_3$ are used; while in the vanadium-organometallic system, $VO(acac)_2$ and $VO(OC_3H_7)_3$ are applied. The details are discussed separately in the following two sections.

2.1.1. Parameters that affect film growth in APCVD system with vanadium halide precursor

The phase diagram plotted by Kang [27] states that the two most critical factors for the composition of produced films is temperature and the ratio of mole fractions for V and O. As described in Fig. 5, it should be noticed that the VO_2 pure phase can be produced at the oxygen mole fraction of 0.66 as marked by the arrow. With the oxygen mole fraction decreasing, triclinic Magnéli phases V_nO_{2n-1} (n = 4, 5, 6, 7, 8) will be formed. Hence, the reaction parameters must be carefully tuned to ensure the correct stoichiometry and phase.

Vernardou et al. conducted a series of experiments in 2006 [65] and 2011 [66] to show the effects of process parameters on the stoichiometry of film by using VCl_4 and H_2O as the precursors with fixed flow rate of 12 L/min. In 2016, Gaskell et al. deposited VO_2(M) on fluorine doped tin oxide pre-coated borosilicate substrate by using the same precursor and fixed flow rate [67]. As summarised in Fig. 6, it shows that when the substrate temperature was higher than 450 °C and VCl_4:H_2O molar ratio was less than 0.5, V_2O_5, as marked in dark cyan region, was formed; while V_2O_3, as circled in purple, was formed when the VCl_4:H_2O ratio was 1 and temperature was up to 450 °C. In contrast, when the temperature was less than 400 °C, in nearly all VCl_4:H_2O ratio region except 0.6, there was no crystalline phase as shown in two olive rectangular boxes. The general trend suggested that with increasing VCl_4:H_2O ratio, the valance of V of the produced decreased. Interestingly, VO_2, as marked in wine-coloured T shape zone, was able to be deposited on SiO_2 buffer layer pre-coated glass at 450–475 °C with a VCl_4:H_2O molar ratio of 0.55–0.8 [65], however by changing different substrates, Gaskell could obtain VO_2 at lower temperature starting from 350 °C by fixing the VCl_4:H_2O molar ratio to 0.6 [67]. The possible reason for this observation remains unknown.

It was found out the flow rate influences the phase formation of vanadium oxide. Fig. 7 summarises the experimental results for both VCl_4-H_2O and $VOCl_3$-H_2O system including the effects of temperature, molar ratio and flow rate. Fig. 7(a) shows the ternary diagram indicating the relationship between film stoichiometry and variation of normalised parameters for both VCl_4 and $VOCl_3$ systems and Fig. 7(b) and (c) are the 3D-XYZ diagram of two different systems respectively for better viewing of the actual experimental conditions. From Fig. 7(a)

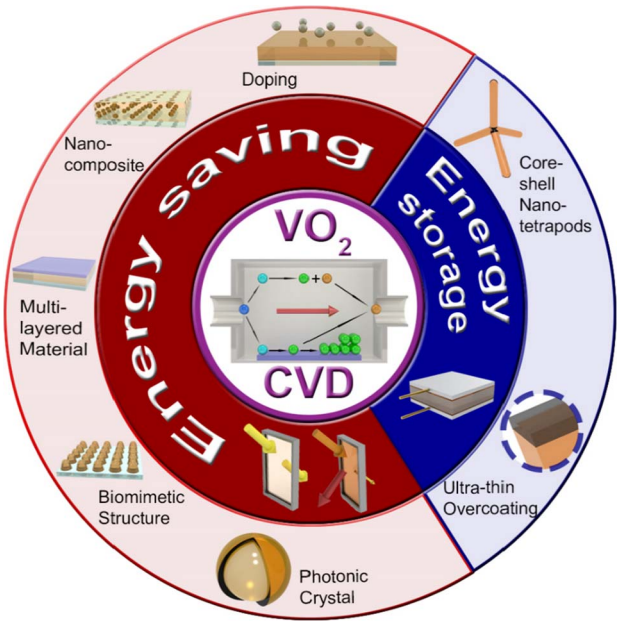

Fig. 2. Strategies that enhance the performance of VO_2 for the energy saving and energy storage applications.

Table 1
Structures and some properties for four major phases of VO_2.[c]

Phase	Lattice	Space group	Application example	Remarks
VO_2(R)[a]	Tetragonal	$P4_2/mmm$	Smart windows coating [57], High damping materials [58], Smart radiator devices for spacecraft [17], Field effect transistors [17], Resistive random-access memories (RRAMs) [59]	Stable from 68 °C to 1540 °C
VO_2(M)	Monoclinic	$P2_1/c$		Stable below 68 °C
VO_2(A)[b]	Tetragonal	$P4_2/nmc$	Unknown	Metastable
VO_2(B)	Monoclinic	$C2_1/m$	Electrode, Supercapacitor	Metastable

[a] VO_2(R) stands for the rutile phase of VO_2, which is produced by phase changing of VO_2(M) when the temperature above 68 °C.
[b] VO_2(A) is the intermediate phase in the phase transition from VO_2(B) to VO_2(R).
[c] The lattice and space group information are summarised from Ref. [60].

and (b), we find that the VO_2 pure phase as shaded in wine-colour region could be deposited at two regions, namely region 1 at 350–475 °C with a VCl_4:H_2O molar ratio of 0.55–0.8 and a fixed flow rate of 12 L/min as well as region 2 at higher temperature (500–550 °C), the richer H_2O supply (VCl_4:H_2O molar ratio from 0.05 to 0.2) and a slower flow rate (~1 L/min). It is worth noting that by adding dopants such as Ti and W, the process condition varied. Specifically, titanium-doped VO_2 was formed with significantly high flow rate (18 L/min), which can be obviously observed in Fig. 7 (b). By increasing substrate temperature and the fraction of V-precursor, V_2O_5 could be formed with flow rate fixed at 12 L/min with an exception when the flow rate reduced dramatically to ~1.5 L/min and decreased temperature from 450 to 475 °C as shown in Fig. 7(b). In the lower flow region, V_6O_{13}, as shaded in navy blue, could be formed with increased VCl_4 concentration compared with V_2O_5.

The use of $VOCl_3$ as a precursor is relatively rare in recent years. By combining Fig. 7(a) and (c), it shows that $VOCl_3$-H_2O system produced V_2O_5 and V_2O_5-V_6O_{13} mixing phase at the temperature 350–600 °C with the $VOCl_3$:H_2O molar ratio from 0.6 to 4 and the flow rate of 1.5–3.5 L/min. The V_2O_5 production region for the $VOCl_3$-H_2O system in Fig. 7(a) was larger than the region of the VCl_4-H_2O system which suggests that V_2O_5 is more readily formed with this precursor. However, no VO_2 pure phase production was observed. The parameters and results differences between VCl_4-H_2O and $VOCl_3$-H_2O system can be explained by the different reaction mechanism. The reaction happened in VCl_4-H_2O system is a simple hydrolysis reaction. In contrast, a reduction-oxidation (redox) reaction happens in $VOCl_3$-H_2O system. Therefore, the VCl_4 system is easier to control than the $VOCl_3$ system and recommended for VO_2 growth.

2.1.2. Parameters that affect film growth in APCVD system with vanadium-organometallic precursor

Similar to the system with vanadium halide, the film stoichiometry in the vanadium-organometallic applied system is affected by temperature, the molar fraction of the precursor, and total flow rate. Vernardou et al. evaluated the influence of variations in conditions on the stoichiometry in the system with $VO(acac)_2$ and oxygen and plotted a binary diagram [65]. As described in Fig. 8, the deposition for $VO(acac)_2$ required a higher temperature compared with the VCl_4 system as explained in Section 2.1.1 and the process window was much wider regarding oxygen flow rate (0.1–0.9 L/min). In $VO(acac)_2$ system, the intramolecular decomposition is the major reaction, while the reaction between VCl_4 and H_2O is a simpler intermolecular hydrolysis reaction.

There are several publications [72–75], which reported successful deposition with $VO(OC_3H_7)_3$ on SnO_2 pre-coated glass, and indium tin oxide (ITO) coated substrate. The growth temperature of these experiments was set in the range of 300–450 °C, which was significantly lower than the optimum growth temperature for $VO(acac)_2$ system (Fig. 8). In two reports [73,75] the stoichiometry of film produced with different carrier gas flow rate through precursor was particularly evaluated. The results showed that in the temperature range of 400–450 °C, VO_2 could produce with the O_2 flow rate in the range of 2–4 L/min.

Similar to halide precursor system, deposition of VO_2 film with vanadium-organometallic was affected by different substrates such as borosilicate glass, fused quartz, (1 0 0) MgO single crystal, (1 0 0) $SrTiO_3$ crystal, (1 0 0) Si wafer, and randomly oriented sapphire [72,74,76]. It has been found that the pure VO_2 was deposited only on fused quartz and sapphire substrate while mixture phases of V_3O_7 or V_4O_9 were formed on other substrates. The difference among substrates could be due to the lattice mismatch and thermal coefficient expansion of VO_2 and substrates.

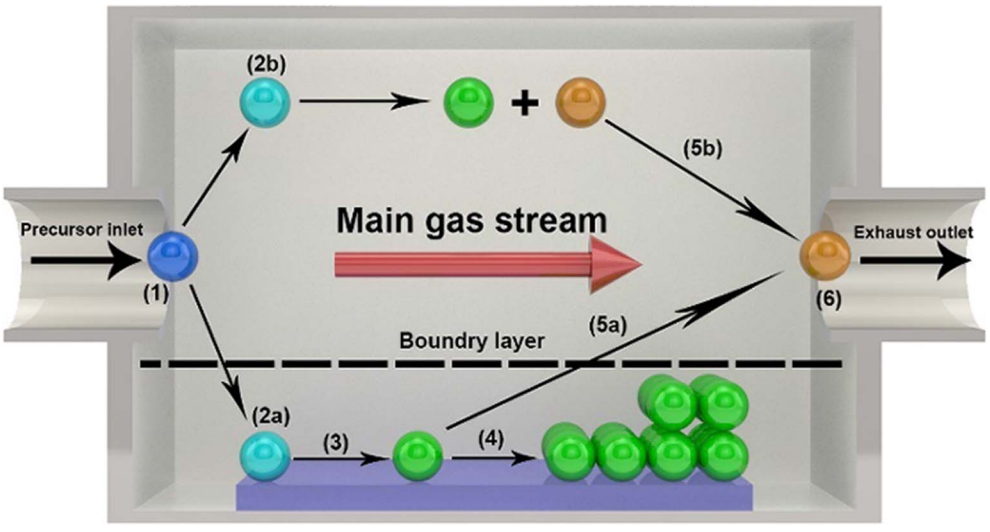

Fig. 3. Schematic diagram of the CVD process: (1) precursor introduction; (2a) precursor absorbing; (2b) homogeneous reaction; (3) heterogeneous reaction; (4) film forming and coalescence; (5a), (5b) by-product transporting; (6) exhausting.

Table 2
Advantages and disadvantages of some commonly used CVD techniques [62,63].

Type of CVD	Advantages	Disadvantages
APCVD	• Fast deposition rate • Good robustness, easy to clean and maintain • Simple system configuration	• Relatively low uniformity and step coverage • Difficult to control film quality and volatile precursor is a must
PECVD	• Good film-substrate adhesion • Able to deposit film at low temperature	• Plasma may damage substrate due to energetic particle bombardment • Complex system configuration • Difficult parameter controlling due to presence of plasma
MOCVD	• Able to control film thickness precisely • Good film quality and uniformity	• Precursor is usually highly toxic • High purity precursor is required • Difficult to get rid of carbon contamination
AACVD	• Fast deposition rate • Capable for non-volatile precursor	• Poor film-substrate adhesion • Relatively high defect density
Hybrid AA/APCVD	• Suitable for composite production	• Complex system configuration • Difficult to control synthesis parameters
ALD	• Precise thickness control • Good uniformity • Low defect density • Able to deposit film at low temperature	• Slow deposition rate • Complex system configuration

2.2. Metal-organic chemical vapour deposition (MOCVD)

The pressure of MOCVD system varies from 1 torr to atmospheric and two categories of precursors are commonly used: (1) β-diketonates such as $VO(acac)_2$, $V(acac)_3$ and vanadyl bis-hexafluoro acetylacetonate $[VO(hfa)_2]$ and (2) alkoxides such as $VO(OC_3H_7)_3$ and vanadyl ethoxide $[VO(OC_2H_5)_3]$ [77]. However, the performance of these precursors is different. Barreca et al. evaluated performances of four kinds of β-diketonates precursors: $VO(acac)_2$, $VO(dpm)_2$, $VO(fod)_2$ and $VO(hfa)_2(H_2O)$ (Note: Hdpm: 2,2-6,6-tetra-methyl-3,5-heptanedione; Hfod:2,2-dimethyl-6,6,7,7,8,8,8-hepta-fluoro-3,5-octanedione) [78]. The first three precursors produced VO_2 in oxygen atmosphere while the last one only produced V_2O_5 in oxygen but could produce VO_2 in a nitrogen atmosphere.

The precursor applied in MOCVD can be in vapour or liquid form. The direct liquid injection MOCVD (DLI-MOCVD) can control film stoichiometry more precisely [79].

2.2.1. Parameters that affect film growth in MOCVD

The film stoichiometry in MOCVD is affected by temperature and the molar fraction of precursor [65] and the molar fraction in MOCVD system is mainly controlled by oxygen flow rate. As shown in Fig. 9, the optimum growth temperature for DLI-MOCVD was 375–475 °C, which was significantly lower than for APCVD (Fig. 8) but DLI-MOCVD seemed to have narrow process window. When the oxygen flow rate was between 0.02 and 0.04 L/min, VO_2(M) single phase was produced at the temperature in the range of 450–475 °C. Furthermore, when the oxygen flow rate was within 0.04 to 0.08 L/min, VO_2(M) and VO_2(B) mixed phase would be deposited at 425 °C. However, if the temperature decreased to 400 °C, VO_2(B) single phase would be produced.

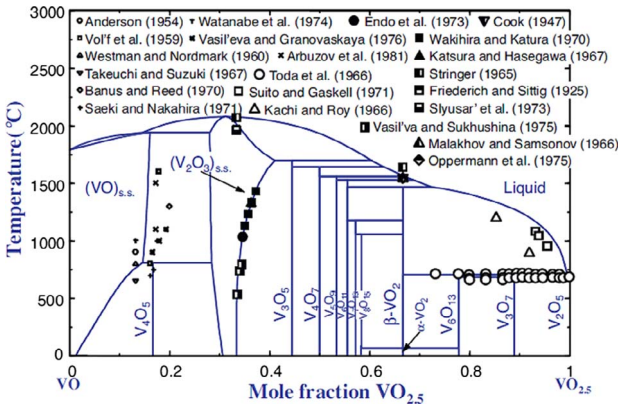

Fig. 5. Phase diagram of VO_x system. The arrows indicate the position of V_2O_3 and α-VO_2. The x-axis represents the mole fraction of $VO_{2.5}$ in the compound. For example, V_2O_5 is considered as $VO_{2.5}$; VO_2 can be regarded as the combination of **33%** of VO and **66%** of $VO_{2.5}$. α-VO_2 stands for VO_2(M), and β-VO_2 refers to VO_2(R). Reprinted from Ref. [27]. Copyright 2012, with permission from Elsevier.

Spanò et al. studied the influence of growth temperature (200–750 °C) on the film morphology and stoichiometry in a 3 torr MOCVD reactor with an oxygen flow rate of 0.15 L/min as shown in

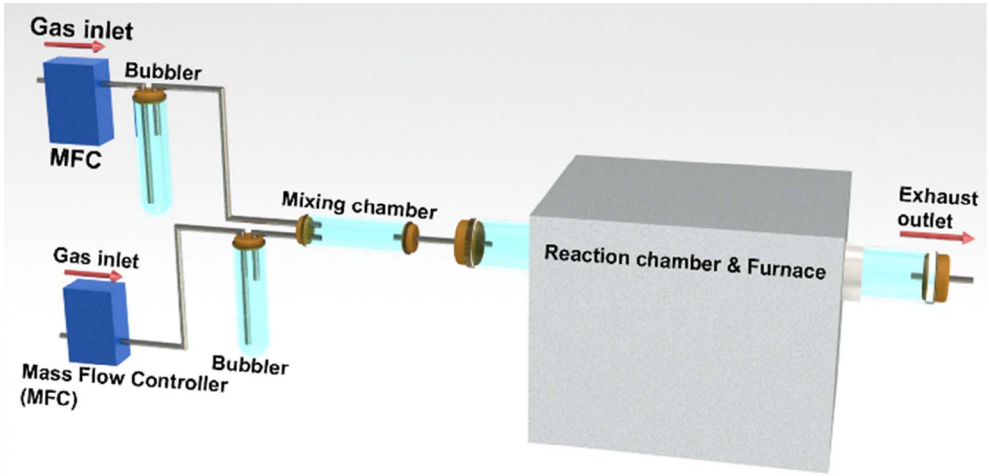

Fig. 4. Schematic diagram for APCVD system.

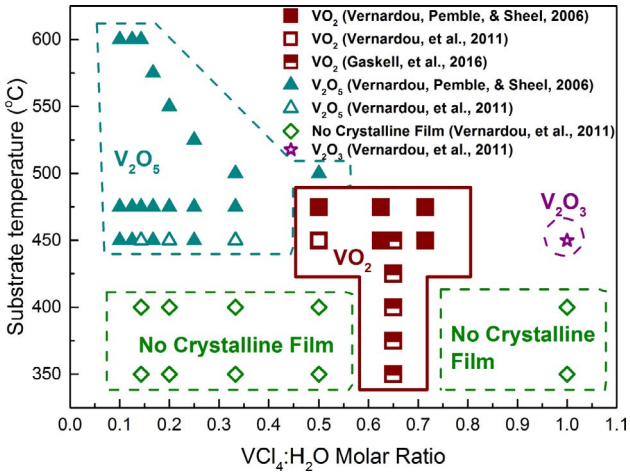

Fig. 6. Binary diagram shows the results of Vernardou's [65,66] and Gaskell's experiments [67].

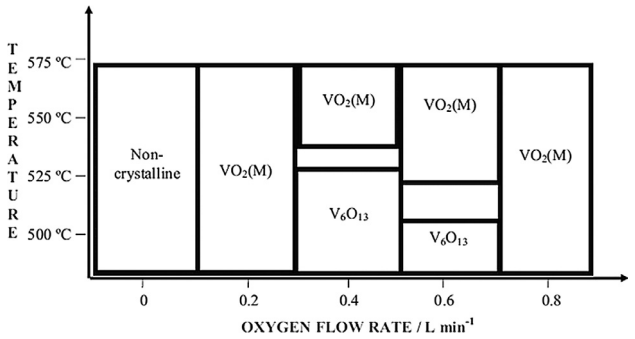

Fig. 8. Influence of oxygen flow rate and temperature on film stoichiometry at a fixed total flow rate of 12 L/min in APCVD. Reproduced from Ref. [65] with permission from Wiley.

Fig. 10 [77]. VO_2 was produced at 200–350 °C, which was lower than Vernardou's experiment (Fig. 9) [65]. During the experiment, when the temperature increased to 400–500 °C, V_6O_{13} was formed. Moreover, V_2O_5 deposition was observed if the temperature was higher than 500 °C. The structure of film growth at 200 °C consisted nanocolumns with the width of 70–80 nm [Fig. 10(a)]. If temperature increased to 300 °C, the plate-like structure appeared and the width kept increasing with increasing temperature [Fig. 10(b)–(f)] [77].

2.3. Plasma enhanced chemical vapour deposition (PECVD)

PECVD has an advantage in thin film deposition compared to the other deposition techniques, as it utilises either a strong electrical field or microwave to produce plasma to decompose precursor and promote film formation which results in lower temperature deposition. However, there are rare reports of VO_2 synthesis with PECVD due to the complexity of the PECVD system. Interestingly, several groups have reported the synthesis of V_2O_5 with vanadium organometallic precursor and oxygen gas [80–82]. The synthesis of V_2O_5 is relatively easy because V_2O_5 is the most thermodynamically stable phase at room temperature. In 1998, Zhang et al. produced vanadium oxide for battery cathode, using $VOCl_3$, O_2 and H_2 as precursors [83]. The radio-frequency power was used to form the plasma with V_6O_{13} thin film

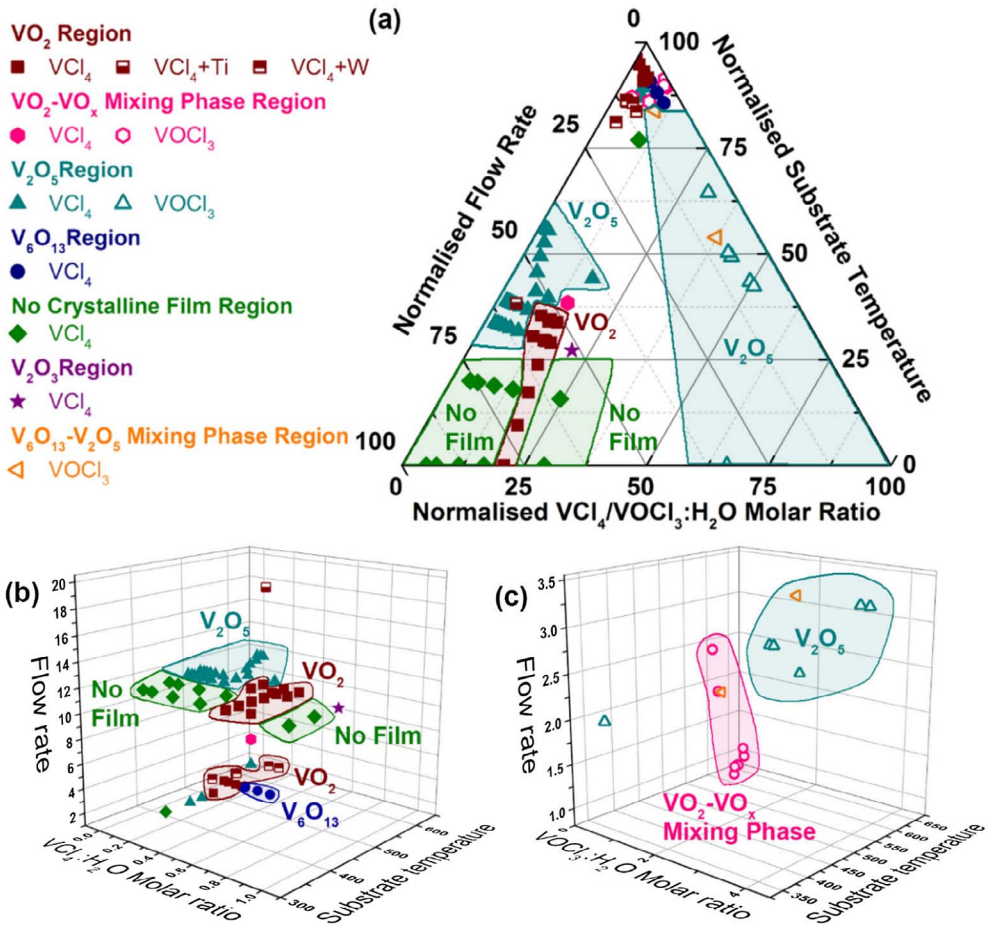

Fig. 7. (a) Ternary diagram shows the relationship between film stoichiometry and variation of normalised parameters in both VCl_4 and $VOCl_3$ systems. (b) 3D-XYZ diagram shows the experiment results for VCl_4 systems. (c) 3D-XYZ diagram shows the experiment results for $VOCl_3$ system. The data of VCl_4 system are collected from Refs. [65–70]. The data of $VOCl_3$ system are collected from Ref. [71].

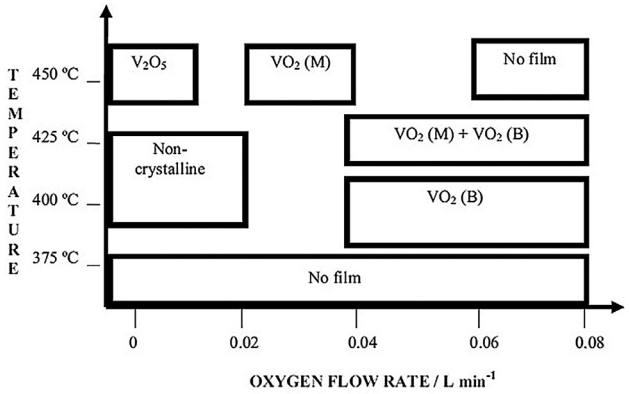

Fig. 9. Influence of oxygen flow rate and temperature on film stoichiometry at a fixed total flow rate of 3 ml/h in a MOCVD system. Reproduced from Ref. [65] with permission from Wiley.

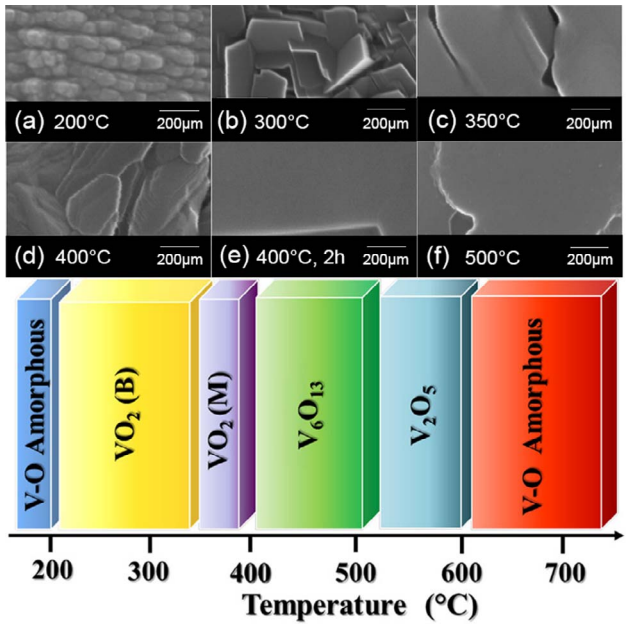

Fig. 10. Morphologies and compositions of film produced at different growth temperatures with MOCVD. Adapted from Ref. [77] with permission from Wiley.

produced, which gave a high discharge capacity of 408 mAh g^{-1}, negligible capacity fading after repeated charging and energy density of 960.3 Wh kg^{-1}. The chemical reactions involved in the synthesis of V_6O_{13} are: $4VOCl_3 + 6H_2 + 3O_2 \leftrightarrow 2V_2O_5 + 12HCl$ and $12VOCl_3 + 18H_2 + 7O_2 \leftrightarrow 2V_6O_{13} + 36HCl$. A similar idea can be used to synthesize VO_2. Since vanadium atoms in VO_2 has a valence number of +4, Zhang's experiment can be modified by selecting precursors with vanadium valence number of +4 or reducing the amount of oxygen so that VO_2 could be produced. Therefore, we recommend employing precursors such as VCl_4 and $VO(acac)_2$ to avoid the possible introduction of an oxidant or reductant.

2.4. Aerosol assisted chemical vapour deposition (AACVD)

AACVD utilises aerosol instead of vapour to produce thin film. Commonly, an ultrasonic humidifier (Fig. 11) is used to generate a precursor aerosol which circumvents the limitation of volatile precursor allowed in APCVD. The aerosol is firstly transported into the reaction chamber as shown in Fig. 11 with the solvent evaporated and remaining precursor particles absorbed onto the substrate followed by heterogeneous reaction. The film is deposited on the substrate, and by-products are desorbed and transferred away from substrate [84].

Naik et al. produced VO_2 pure phase with $VO(acac)_2$ single precursor via AACVD [85]. The precursor was dissolved in ethanol and formed aerosol by an ultrasonic humidifier. Nitrogen gas served as carrier gas in the experiment. The VO_2 pure phase was produced at 450–600 °C with an island growth morphology. Besides $VO(acac)_2$, commonly used precursors for AACVD includes $V(acac)_3$ [86] and other kinds of organic metal oxide.

The effects of external electrical field to the morphology of VO_2 film were extensively researched [87–92]. The applying of electrical field decreased the average particle size, increase the film porosity, enlarge the surface area but more prone to oxidation [93].

AACVD has some limitations such as poor adhesion between film and substrate, and relatively high defect density [61]. Those limitations might be due to the rapid deposition speed. Since a large number of the particles are deposited on the substrate in short time, they do not have enough time to diffuse and re-arrange themselves to the lower energy growth site.

2.5. Hybrid AA/APCVD

Hybrid AA/APCVD combines the systems and advantages of both AACVD and APCVD as shown in Fig. 12. This system can deposit film with high quality and uniformity. At the same time, it can add nanoparticle into film by using nanoparticle slurry aerosol. Hybrid CVD method is suitable for producing nanocomposite.

Warwick et al. produced the plain VO_2 thin film, VO_2-TiO_2 nanocomposite and VO_2-CeO_2 nanocomposite by hybrid CVD (Fig. 13) [94]. The VO_2 film was synthesised with $VO(acac)_2$ and oxygen. $VO(acac)_2$ was heated in the bubbler and carried by nitrogen-oxygen mixture gas into the reaction chamber. At the same time, nanoparticles were transported into the chamber in the form of aerosol. All the composites showed reduced τ_c compared with bulk VO_2, and the reflectance showed a significant change of 30% between at 25 °C and 80 °C. The films had the photocatalytic properties similar to titanium dioxide thin film. The group concluded that although the T_{lum} of the nanocomposite was still needed to be improved, hybrid CVD is a promising way to produce thermochromic nanocomposite.

2.6. Atomic layer deposition (ALD)

ALD is an “extreme” case of CVD. It utilises self-terminating surface half-reactions to control deposition. Since only a single molecular layer is formed in one cycle, ALD can form a very high-quality thin film with precise thickness control. The reaction cycle must be repeated for several times to deposit thicker film, which makes ALD a slow and high-cost CVD technique. Tetrakis[ethylmethylamido]vanadium (TEMAV) is the vanadium contained precursor commonly used in ALD [95–99]. Other precursors used in ALD include $VO(OC_3H_7)_3$ [100] and $VO(acac)_2$ [101]. The common oxygen source used in ALD includes water [100], ozone [99,102] and oxygen plasma [103].

The self-terminating surface half-reaction is the foundation of ALD process. Factors such as reaction temperature, precursor injection time and purging time have to be carefully tuned in order to achieve this reaction. To form a saturated monolayer, the binding energy between substrate and precursor should be larger than the binding energy between the monolayer and precursor particles above [104]. Therefore, a precise temperature controlling is required. As the amount of injected precursor has to be in excess to ensure that a saturated layer is formed, an adequate purging time is needed for the excess precursor to evacuate the reaction chamber. The report of Rampelberg et al. demonstrated a typical ALD process for VO_2(M) film deposition at 150 °C with TEMAV and O_3 as precursors as shown in Fig. 14 [99]. Firstly, TEMAV was introduced into the system to form multilayers followed by purging and re-evaporation of excess precursors to ensure the monolayer formation. O_3 was introduced into the system and reacted with TEMAV; the

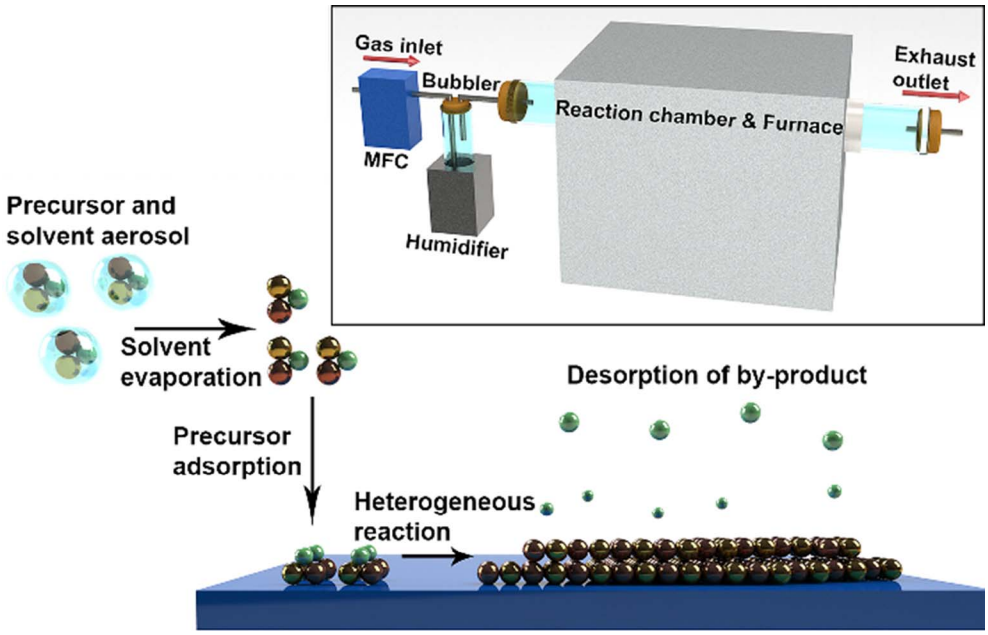

Fig. 11. Mechanism and system configuration for AACVD.

unreacted O_3 was purged out of the chamber. An amorphous VO_2 film was produced and then was subsequently annealed at 450 °C in a He atmosphere for 30 min to form VO_2(M) phase.

The parameters of different CVD to produce VO_2 is summarised in Table 3. It can be seen that vanadium-organometallic precursors such as $VO(acac)_2$ and $VO(OC_3H_7)_3$ have the largest process window for APCVD, MOCVD and AACVD system, which are especially suitable for the system with rough condition controlling. VCl_4-H_2O system can deposit pure phase VO_2 with little contamination but because of its high toxic and narrow process window, it highly recommends establishing an APCVD system with good sealing and precise condition controlling when applying this precursor. TEMAV is the precursor with the lowest reaction temperature. Although currently it is only used for ALD, the precursor has high potential to be used in other CVD techniques such as MOCVD and AACVD. The least used precursor $VOCl_3$ is not recommended because of the difficulty to produce VO_2 pure phase and the highest reaction temperature among precursors.

3. Strategies used in CVD system for improving VO_2 film's energy conservation performance

3.1. Doping

VO_2 application in thermochromic smart window is limited by high τ_c and doping is the effective way to reduce τ_c. We summarised the effect of various dopants on the thermochromic performance in Table 4. Only a few elements have been doped using CVD, including W, F, Mo and Nb. Tungsten is an extensively used dopant for VO_2 due to its effectiveness in reducing τ_c [105]. Commonly used W-contained precursors include WCl_6 [106–108], $W(OC_2H_5)_6$ [107] and $W(OC_2H_5)_5$ [109,110]. As the Table 4 and Fig. 15(c) describe, W has the most outstanding effect of τ_c decreasing among the dopants and the τ_c decreasing effect is linearly related to the W concentration. Despite the effectiveness of decreasing τ_c, W doping has the shortcomings to reduce T_{lum} and ΔT_{sol}.

Other dopants such as Mo, Nb and F encountered the same problem (Table 4): They can only improve either one or two properties of VO_2. For example, Nb decreased τ_c, T_{lum} and ΔT_{sol} at the same time [111]. F could only increase T_{lum} but broaden the hysteresis loop width at the same time [112,113]. Although Mo was able to decrease τ_c and increase T_{lum} at the same time, the reduction of Mo ion during CVD limited the effect of performance optimising [114].

Two remedies namely discovering new dopants and co-doping were employed to meet the challenge of decreasing τ_c and increasing T_{lum} and ΔT_{sol} at the same time. Several new dopants such Mg, Zr and rare earth elements like Eu, Tb and La can reduce τ_c, enhance T_{lum} and ΔT_{sol} at the same time (Table 4). It is worthwhile to employ CVD to dope such elements in future as CVD is a gas phase process which can facilitate the

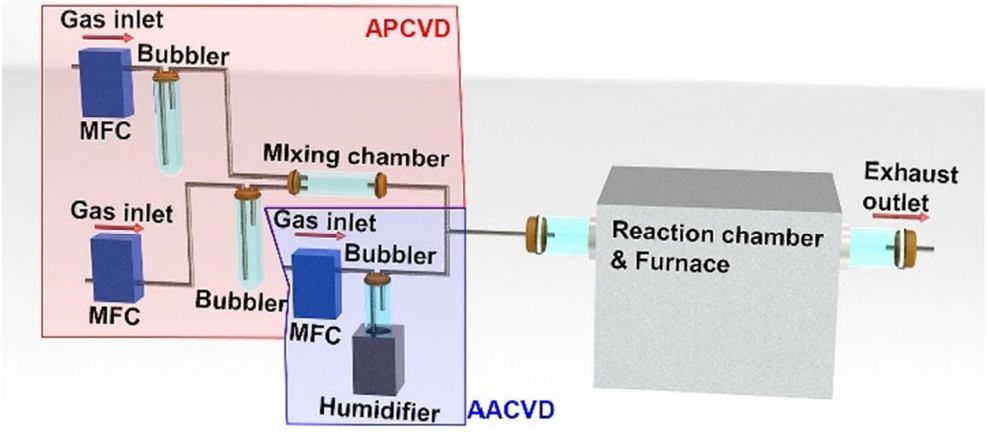

Fig. 12. Schematic diagram for hybrid AP/AACVD.

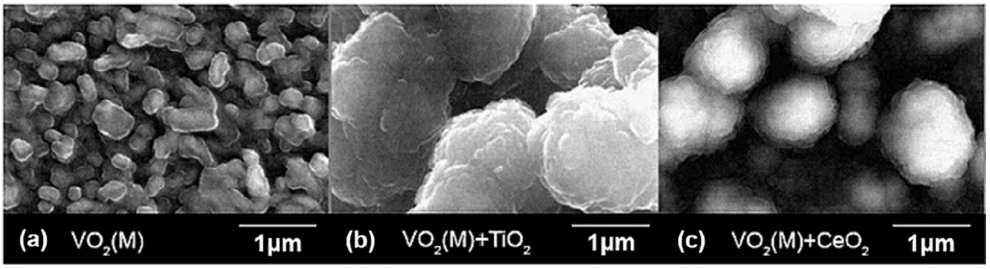

Fig. 13. Scanning electron microscope (SEM) image for (a) plain VO_2 thin film, (b) VO_2-TiO_2 nanocomposite and (c) VO_2-CeO_2 nanocomposite. Reprinted from Ref. [94]. Copyright 2011, with permission from Elsevier.

doping effectiveness.

On the other hand, co-doping is a more time-saving strategy since it improves VO_2 properties by combining the strength of currently available dopants and avoids their shortcomings. Some groups reported promising performance improvement by W/F co-doping [115] and W/Mg co-doping [119] and rare-earth/W co-doping [136]. The W/Mg co-doped sample prepared by Wang et al. via dip coating with V_2O_5, H_2O_2, Mg and W powder showed a decreased τ_c (~35 °C) and an outstandingly high T_{lum} (81.3%) which was one of the highest T_{lum} among the reported cases [119]. Since CVD is a method that especially suitable to produce doped uniform thin film due to its mechanism and system configuration, co-doping is a future research topic with high potential and application value for CVD.

3.2. Forming of composite materials

CVD is suitable to produce certain types of composite materials: AACVD and hybrid AP/AACVD are good at producing nanocomposite and mixing phase materials since they can distribute nanoparticles and different phases in the matrix evenly. Conventional APCVD, MOCVD and ALD are more suitable to produce multi-layered structure materials and template assisted growth of biomimetic and photonic structure due to their ability to deposit high-quality thin film.

Gold/VO_2 nanocomposite is the most intensively studied form of nanocomposites due to the surface plasmon resonance (SPR) of gold nanoparticles and the changing of optical performance introduced by SPR [137]. Several groups reported the preparation of gold/VO_2 nanocomposite with $HAuCl_4$ as (gold) Au provider via hybrid AP/AACVD, the observation of a film colour changing (from a brown colour to blue-green colour) [109] and τ_c decreasing (~42 °C) [138]. The influence of SPR to the optical and thermochromic properties of VO_2 requires future detailed investigate. Since the size and shape of nanoparticle can directly affect the SPR effect, the formation of nanocomposite with different particle size and shape, nanocomposite performance characterisation and structure optimising are attractive topic to research. Furthermore, because other precious metal such as Ag also has SPR effect, the nanocomposite between VO_2 and other precious metals and its performance is an interesting topic to be discovered.

Mixing phase is a reliable way to prepare multi-functional materials. Some groups produced multi-functional material that combined the photocatalytic properties from TiO_2 and thermochromic properties from VO_2 via APCVD or hybrid AP/AACVD with $TiCl_4$ [69,139] or Ti(O^iPr)$_4$ [140]. All samples in those cases showed a decreased τ_c at ~50 °C with a promising photocatalytic effect.

Multi-layer structure is an effective way to produce high-performance or multifunctional materials. Liu et al. produced VO_2 thin film with enhanced T_{lum} and ΔT_{sol}, promising hydrophobicity and anti-oxidation ability by coating a Si-Al based anti-reflecting layer (AR-layer) via sol-gel method [18]. Meanwhile, Evans et al. prepared TiO_2/VO_2 multilayer samples with different structures (TiO_2 on VO_2 and VO_2 on TiO_2) and observed that the morphology of both composites was dominated by TiO_2 (Fig. 16) [141]. Moreover, the TiO_2 on VO_2 sample

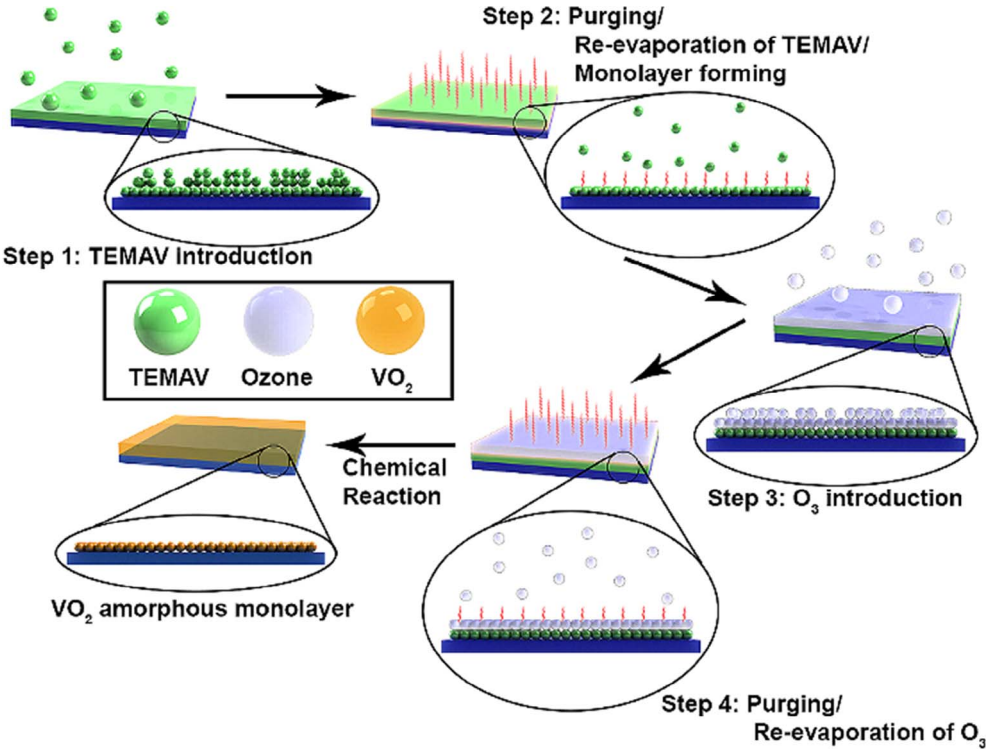

Fig. 14. Schematic diagram showing the ALD process reported in Rampelberg et al. [99]'s case.

Table 3
Precursor and parameters for various CVD techniques to deposit pure phase VO_2(M), pure phase VO_2(B), mixture of VO_2(M) and VO_2(B) and VO_2-VO_x mixing phase.

Method	Precursor/Results	Controlling			Remarks
		Molar ratio	T (°C)[a]	Flow rate (L/min)	
APCVD	VCl_4-O_2[b]	0.45–0.8	350–475	12	• Able to produce pure VO_2 phase with little contamination
		0.05–0.2	500–550	0.5–1	• Recommend for the system with precise condition controlling.
	$VOCl_3$-O_2/Mixing phase	0.5–1	600–650	0.5–2.5	• Produce mixing-phase only
					• Not recommended.
		O_2 Flow rate (L/min)	T (°C)	Total flow rate (L/min)	• Wide process window
					• Recommend for the system with rough condition controlling
	$VO(acac)_2$-O_2/VO_2(M)	0.1–0.9	475–575	12	• Have potential carbon contamination, which may affect optical properties.
	$VO(OC_3H_7)_3$-O_2/VO_2(M)	0.6	300–450	0.7–0.8	
		Precursor flow rate (L/min)	T (°C)	Total flow rate (L/min)	• Able to produce VO_2 film with the single precursor
					• Suitable for the application with low purity requirement
	$VO(OC_3H_7)_3$/VO_2(M)	2–4	400–450	12	• Relatively simple system configuration.
MOCVD		P (torr)	T (°C)	Injection rate	O_2 flow rate (L/min)	
	$VO(acac)_2$-O_2/VO_2(M)	760	430–475	3 ml/h	0.02–0.04	• Wide process window
		3	300–350	0.15 L/min	0.15	• Able to control reaction conditions more precisely than APCVD
	$VO(acac)_2$-O_2/VO_2(M) + VO_2(B)	760	410–430	3 ml/h	0.04–0.08	
	$VO(acac)_2$-O_2/VO_2(B)	760	380–430	3 ml/h	0.04–0.08	
		3	200–300	0.15 L/min	0.15	
AACVD		Solvent		T (°C)	Flow rate (L/min)	• High deposition rate but relatively poor quality
	$VO(acac)_2$/VO_2(M)	Ethanol		450–600	1.5	• Suitable for the applications with low film quality requirement.
	$V(ACAC)_3$/Mixing phase	Ethanol		500–600	1.5	
ALD		P (torr)		T (°C)	Pulse plan (s)[c]	• Precise control of film thickness but complex system
	TEMAV-O_3/VO_2(M)	7.5×10^{-7}		150	2-25-5-15	• Suitable for the application with high requirement to film thickness.
	$VO(acac)_2$-O_2/VO_2(M)	10		400–475	4-2-1-1	• TEMAV is especially suitable for application requires low process temperature.

[a] "T" stands for growth temperature; "P" stands for chamber pressure.
[b] Due to the lack of phase information in some of the reference, we cannot differentiate the optimum conditions for VO_2(M) and VO_2(B) in VCl_4-H_2O system.
[c] Pulse plan describes the purging step in ALD. The four values indicate the time for metal precursor injection, first purging, oxygen/ozone injection and second purging.

Table 4
Effect of dopants on the thermochromic performance of VO_2 films.

Dopant	τ_c[a]	T_{lum}	ΔT_{sol}
W^{6+} [105,115,116]	↓ (~20–26 °C per at.%)	↓	↓
Ti^{4+} [117,118]	↑	↑	↑
Co^{2+} [119]	↓	n.a.	n.a.
Ta^{5+} [119]	↓	n.a.	n.a.
Nb^{5+} [111,120,121]	↓ (~2 °C per at.%)	↓	↓
Mo^{6+} [120,121]	↓ (~3 °C per at.%)	↑	↓
Cr^{3+} [122]	↑	↑	↓
Sn^{4+} [123]	↑ (~1 °C per at.%)	n.a.	n.a.
Al^{3+} [124]	↓ (~2.7 °C per at.%)	n.a.	n.a.
Fe^{3+} [125]	↓ (~6 °C per at.%)	n.a.	n.a.
Ce^{3+} [126]	↓ (~4.5 °C per at.%)	n.a.	n.a.
P^{3-} [127]	↓	n.a.	n.a.
Sb^{3+} [128]	↓	↑	n.a.
Tb^{3+} [129]	↓	↑	↑
La^{3+} [130]	↓ (~1.1 °C per at.%)	↑	↑
Eu^{3+} [131]	↓ (~5 °C per at.%)	↑	↑
Mg^{2+} [14,132–134]	↓ (~3 °C per at.%)	↑	↑
Zr^{4+} [135]	↓ (~0.4 °C per at.%)	↑	↑

In the table, "↑" and "↓" stand for the positive and negative effect on the properties respectively and "n.a." stands for data not available.
[a] The data in the brackets stand for the decreasing of τ_c per at.% of dopant adding.

showed the thermochromic and photocatalytic properties from both VO_2 and TiO_2 but the sample of VO_2 on TiO_2 did not show any photocatalytic effect and τ_c decreasing. Recently, Breckenfeld et al. partially explained the reason behind this phenomenon [142]. As reported by the researchers, the thermochromic properties of VO_2 on TiO_2 is affected by the epitaxial strain due to the lattice mismatch between these two crystals. Epitaxial strain helps to reduce the τ_c by introducing lattice instability. However, if the VO_2 layer is too thick, misfit dislocations will occur and relax the accumulated epitaxial strain. The group proposed a way to solve this problem: carefully choosing the crystal growth direction of both TiO_2 and VO_2, and then annealing the composite to inhibit the generation of misfit dislocation. CVD (especially MOCVD) is good at growing the crystal with certain growth direction. Moreover, unlike other methods such as PLD, sputtering and solution based method, it is possible to anneal the sample without taking it out of the chamber using CVD, which prevents the sample from potential contamination and protects the good quality of the sample.

3.3. Template-assisted growth

Biomimetic structures enhance the thermochromic performance of VO_2 film since the sub-wavelength moth-eye structures provide a continuous refractive index gradient between the air and the medium, which effectively decreases the reflections by reducing the refractive index gap on the air-medium interface. The simulation conducted by Taylor et al. [143] [Fig. 17(a)–(c)] and the sample prepared by Qian et al. [17] via templated assisted sol-gel method [Fig. 17(d)–(h)] confirmed the ability of biomimetic structures to enhance T_{lum} and ΔT_{sol} as showed in Fig. 17(i) and (j). Compared with the sol-gel method, CVD especially APCVD and MOCVD have the advantage to deposit high quality and uniformity film on the complex geometry surface. Therefore, producing the biomimetic structure via CVD and its performance evaluation is an attractive future research topic.

Photonic crystal is one of the promising structures to display conspicuous structural colour due to its photonic bandgap generated by coherent optical diffraction. Ke et al. produced two-dimensional SiO_2-VO_2 core-shell thermochromic photonic sphere via template-assisted sol-gel process [Fig. 18(a)] [55]. The simulation results [Fig. 18(b)] and the experiment results [Fig. 18(c)] both indicated that such structure could achieve both diameter-dependent colours and reliable thermochromic performance. However, because the sol-gel method was not good at preparing high uniformity film with good complex geometry

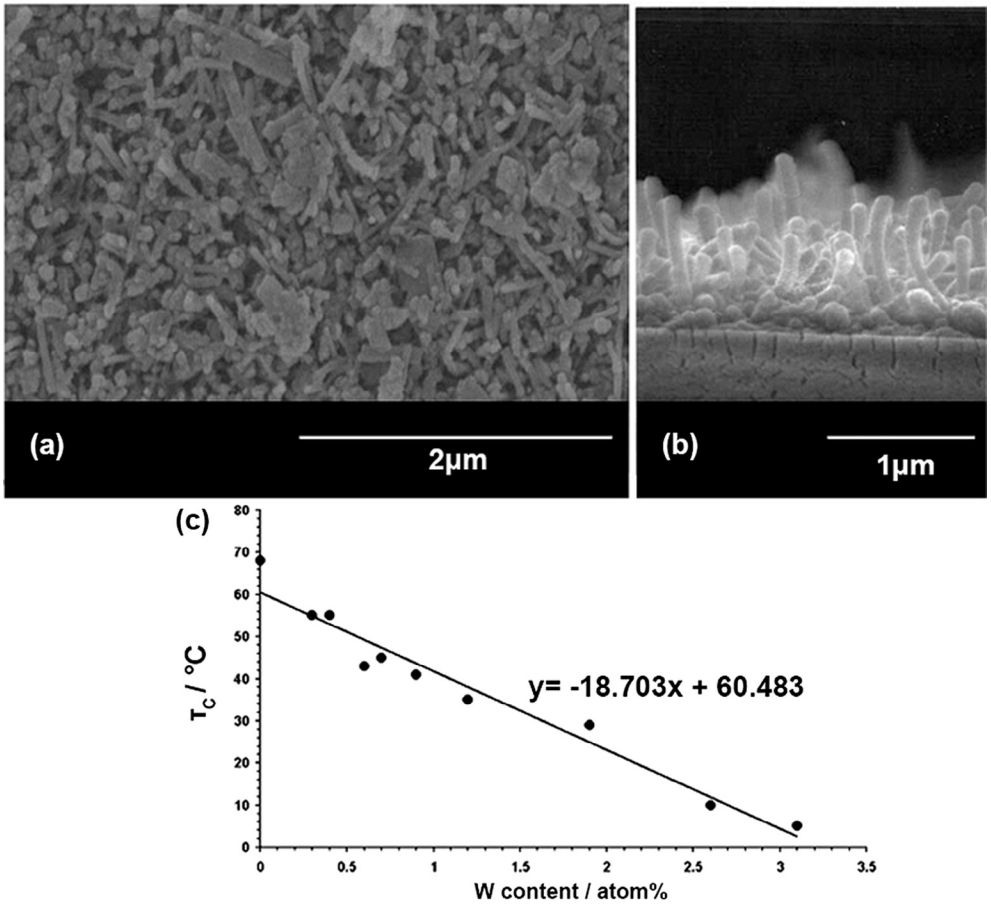

Fig. 15. SEM image from (a). top down and (b) cross-section view of $V_{0.988}W_{0.012}O_2$ film produced by APCVD showing the worm-like structure. (c) Plotted relationship between W concentration and measured τ_C in the experiment. Adapted from Ref. [107] with permission from The Royal Society of Chemistry.

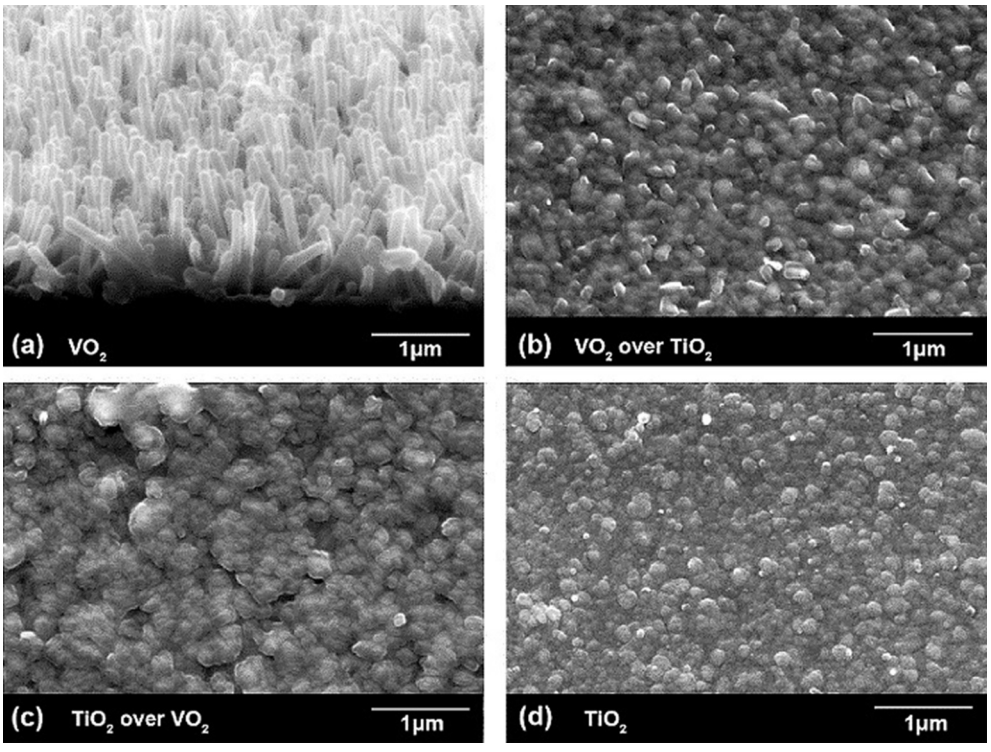

Fig. 16. SEM images of (a). VO_2; (b). VO_2 on TiO_2; (c). TiO_2 on VO_2; (d). TiO_2. Two composites had morphologies that were similar to TiO_2. Reprinted from Ref. [141]. Copyright 2007 with permission from Elsevier.

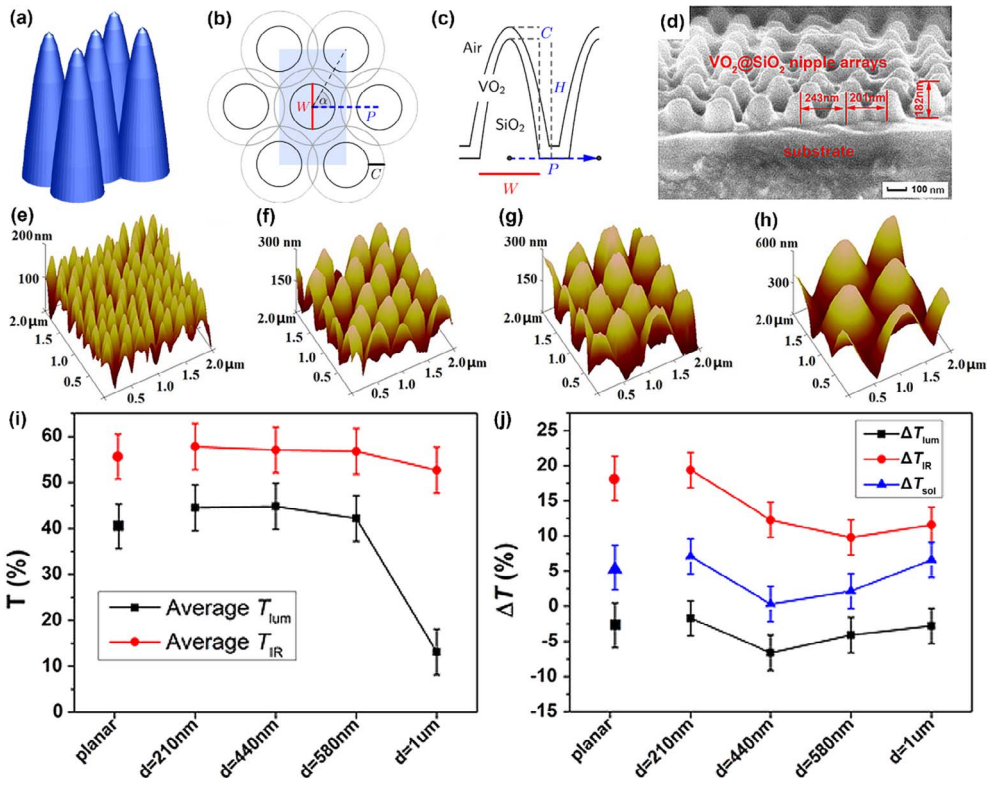

Fig. 17. (a) 3D illustration of nanotextured surface with nipple arrays. (b) Side and (c) top views of hexagonally arranged circular paraboloid cones. (d) SEM cross-sectional profile of the moth-eye nanostructured VO_2 film. AFM analyses of the biomimetic VO_2 films with varied moth-eye structure size of (e) 210, (f) 440, (g) 580, and (h) 1000 nm. Effects of the moth-eye structure size on (i) ΔT_{lum}, ΔT_{IR}, and ΔT_{sol} as well as on (j) T_{lum} and T_{IR}. (a)-(c) are adapted from Ref. [143] with permission. Copyright 2013 The Optical Society. (d)-(j) are adapted from Ref. [17] with permission. Copyright 2014 American Chemical Society.

coverage, the actual T_{lum} and ΔT_{sol} was slightly derivate from the simulated values. CVD as a technique that good at producing coating with good coverage can solve the issue encountered in Ke's experiment. Recently, Ke et al. applied the same method to produced various nanopatterns [144], which also provided ideas for energy saving applications.

4. Strategies used in CVD system for improving the energy storage performance of VO_2 film

4.1. Growth of core-shell structure

In 2014, Yin et al. produced VO_2 coated ZnO nanotetrapods via

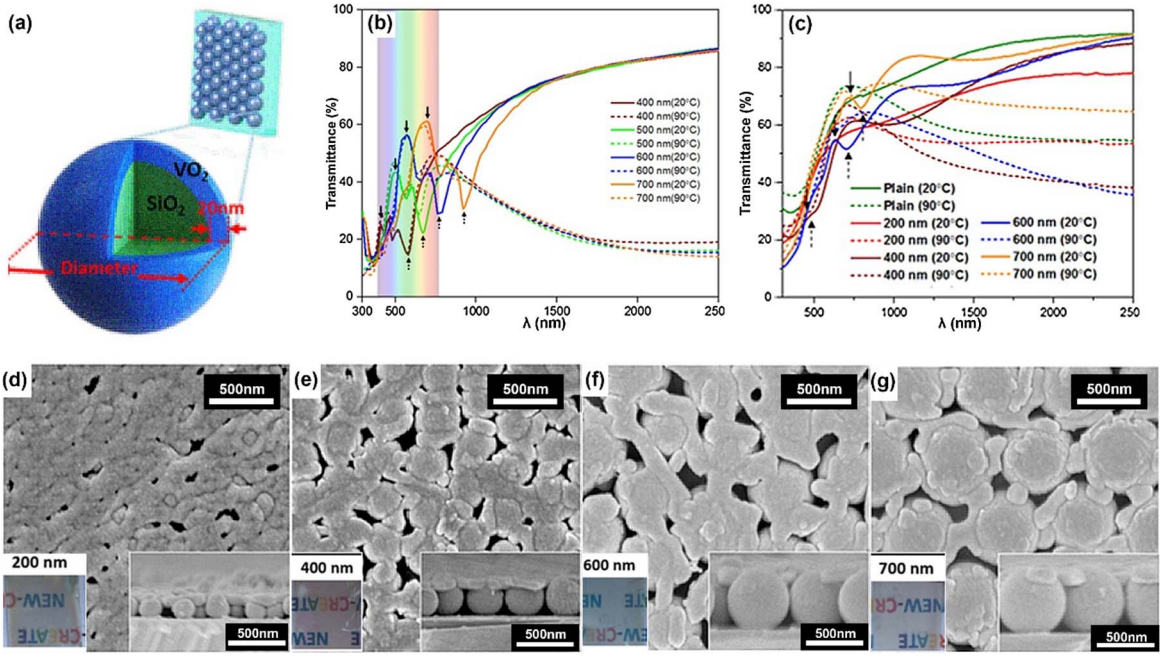

Fig. 18. (a) Illustration of the two-dimensional SiO_2-VO_2 core-shell photonic structure on glass. (b) Calculated transmittance spectra of these structures with diameters of 400, 500, 600, and 700 nm, respectively. (c) Measured transmittance spectra of the structures with silica sphere sizes of 200, 400, 600, and 700 nm, respectively, as well as the plain VO_2 film which serves as a control sample. The transmittance peaks and troughs are indicated by the solid and dashed arrows, respectively. (d-g) Top-view and (bottom-right insets) side-view SEM images of colour-changed samples using silica spheres with diameters of (d) 200, (e) 400, (f) 600, and (g) 700 nm, respectively and (inserted photographs on the bottom left) their corresponding normal-view appearance under sunlight. Adapted from Ref.[55] with permission. Copyright 2016 American Chemical Society.

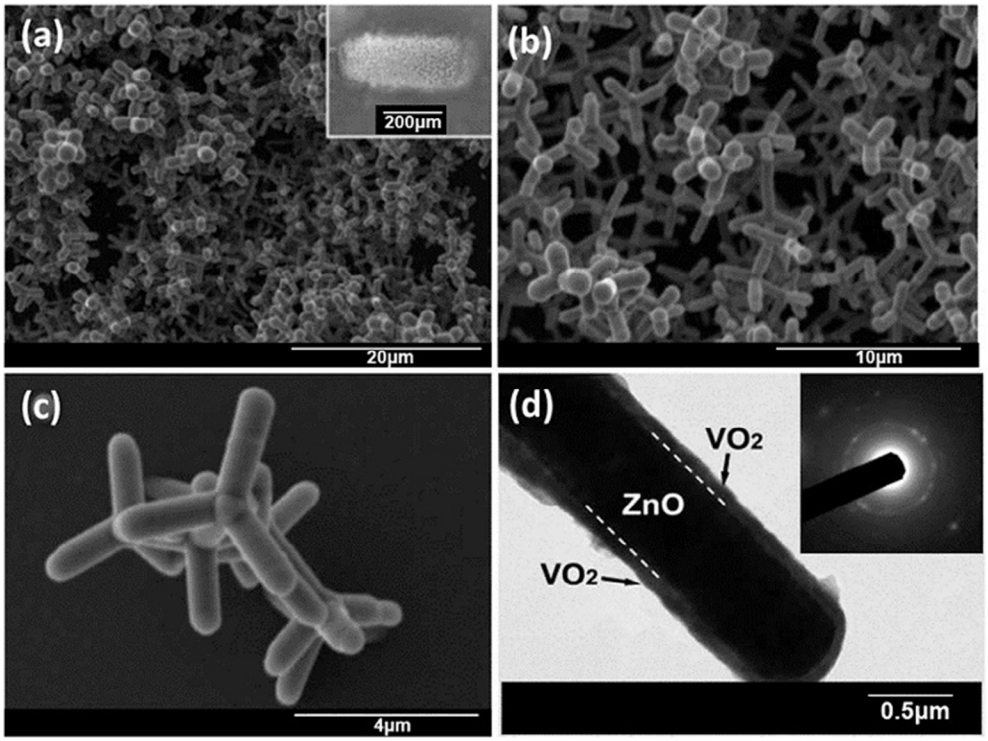

Fig. 19. (a). Low-, (b). medium-, and (c). high-magnification SEM images of VO_2-ZnO core-shell structure; (d) High-resolution transmission electron microscope (TEM) image of a single nanorod of a tetrapod; Upper inset in (d) is the corresponding SAED pattern. Adapted from Ref. [145] with permission from The Royal Society of Chemistry.

APCVD with the precursors of $VO(acac)_2$ and N_2/O_2 mixing gas (Fig. 19) for field emission device applications [145]. The group employed ZnO as skeleton to overcome the difficulty of form VO_2 pure phase nanostructure due to its nonstandard vapour-liquid-solid (VLS) mechanism. The core-shell structure sample showed a temperature dependent field emission property, which had a higher field emission density with the temperature increasing and the temperature dependent property could be attributed to the VO_2 shell. The composite had a better field emission performance than VO_2 pure phase. This case is a good example of applying CVD to produce complex geometry composites and the idea of this case is useful for similar topic in future.

4.2. Morphology modification by changing growth parameter

Vernardou et al. deposited VO_2(B) films with different morphologies by controlling gas flow rate passing through precursor [146]. With an increase in the carrier gas flow rate, the film surface was smoothened, and the size of nanocrystal was decreased. The electrochemical properties of the film showed a negative relationship with the flow rate: the sample prepared with the lowest flow rate (1 L/min) had a specific discharge density of 425 mAh g^{-1}, with a capacitance retention of 97% after 500 cycles of charging (Fig. 20). Porous thin films would allow easy access and wetting by the electrolyte which would increase the ion diffusion kinetics and improve the cycling stability, especially in supercapacitor electrodes. Utilizing the AACVD method, Warwick et al.

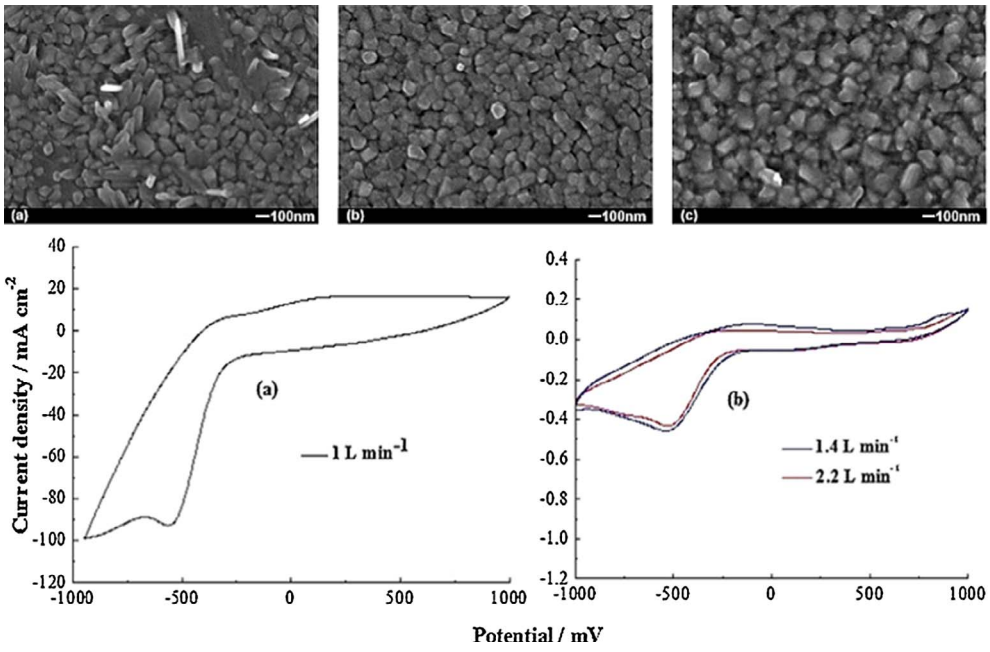

Fig. 20. Field emission scanning electron microscope (FESEM) images and cyclic voltammograms of APCVD vanadium oxide coatings at 500 °C for (a) 1; (b) 1.4; and (c) 2.2 L/min N_2 flow rate through the vanadium precursor bubbler. Reproduced from Ref. [146] with permission from Wiley.

synthesised highly porous VO_2(m) thin films and the crystallite size and porosity of the films can be controlled by varying the deposition time and electric field strength. The sample with small crystallite size, high porosity and best wetting properties displayed a specific capacitance of 3700 μF cm^{-2} and stable cycling performance up to 1000 charge/discharge cycles [147].

4.3. Carbon/VO_2 heterostructure for battery and supercapacitor applications

Carbon/VO_2 heterostructures have drawn attentions as electrode materials for batteries and supercapacitors due to the combination of the good electrical conductivity of carbon and the high specific capacitance/lithium diffusion efficiency of VO_2. Rui et al. synthesised ultra-thin [approximate coating thickness ~ 4.3 nm, as shown in Fig. 21(d)] amorphous carbon coated VO_2 (B) belt via hydrothermal method for battery applications [Fig. 21(a)–(c)] [148]. The ultra-thin carbon coating improved the electronic conductivity without blocking the lithium diffusion pathway. Compared with samples with different concentrations, the sample with 6.6 wt% of carbon showed a balance between conductivity and lithium diffusion efficiency and the overall best charging rate capability compared to the other samples. Other heterostructure battery electrode materials that have been researched recently include graphene quantum dot coated VO_2 arrays [149] and VO_2(B) coated carbon fiber cloth [150]. Both materials showed good specific capacity, fast charging rate at high current density and excellent cycling durability. Moreover, the two structures showed more attractive properties such as flexibility and good compatibility for both Li-ion and Na-ion battery.

On the other hand, heterostructures have also been intensively researched for supercapacitors. The structures for supercapacitor include graphene/VO_2(B) nanosheet composite hydrogel [151], VO_x overcoated carbon nanotube (CNT) structure [152] and VO_2 nano-sphere decorated CNT heterostructure [153]. It is worth noting that researchers have employed CVD to produce VO_x overcoating and VO_2 nanospheres, which proves CVD's capability for producing delicate nanoscale structures [153].

Table 5 summarised the strategies for improving the thermochromic and electrochemical performance discussed in the previous two chapters of the report, and the recommended CVD method for different strategies. As stated previously, APCVD is good at producing the high-quality thin film with accurate stoichiometry control and suitable for the applications required good covering and specified composition. AACVD and Hybrid AA/APCVD are suitable for mixing second phase into the matrix to produce composite materials. ALD is specialised in producing ultra-thin film with good quality.

5. Conclusion and perspectives

5.1. Conclusion

This review discussed various CVD techniques and strategies to produce VO_2 polymorph thin films for energy storage and saving applications and their performances are largely determined by the crystallinity, phase and morphology. In the vanadium-oxygen system, the stoichiometry and the performance of the product are influenced by several parameters such as substrate temperature, the molar ratio of precursor and total flow rate. A ternary diagram and two 3D diagrams were plotted in relation to the phase and stoichiometry of thin film in APCVD system with vanadium halide precursor. The effects of processing condition on the film's quality in other CVD systems were discussed in detail. We reviewed some strategies to improve VO_2 thin film performance for both energy conservation and storage applications respectively. Three approaches, namely doping, composite forming, and template assisted growth to improve VO_2's thermochromic performance further and add multifunction into the smart window system. Meanwhile, the electrochemical performance of VO_2 could be improved by forming core-shell structure material via template-assisted growth, modifying film morphology and forming carbon/VO_2 heterostructure. In summary, CVD is a promising technique to produce high quality and highly uniform VO_2 thin film with different morphology in large scale. This article can serve as a guideline for process control and performance enhancement in both energy conservation and storage applications.

5.2. Future research directions

Although VO_2 has been intensively researched for several years, there is still a long way to go before the commercialization and mass production of the final optimised product for thermochromic smart window and energy storage applications.

In the field of energy conservation, improving the thermochromic performance of VO_2 still remains a significant challenge. Currently τ_c at near room temperature can be achieved through doping and increasing T_{lum} and ΔT_{sol} can be achieved through different methods such as nanopatterning, nanogridding and multi-layered materials. However, the three key requirements namely lower τ_c and enhanced T_{lum} and ΔT_{sol} need to be improved simultaneously. Future research efforts should take this into consideration. Besides, multifunctional thermochromic device is vital for the next-generation energy conservation smart window. Lastly but most importantly, although VO_2 has been successfully deposited on large area, the batched production of VO2 based energy saving materials is currently still in exploration. The low-cost production of VO_2 based smart-window or window coating is highly sought after by both academia and industry, as they may hold great economic potential for commercialisation.

In the field of energy storage, current research is focussed on improving the electrochemical performance of VO_2 electrodes for battery

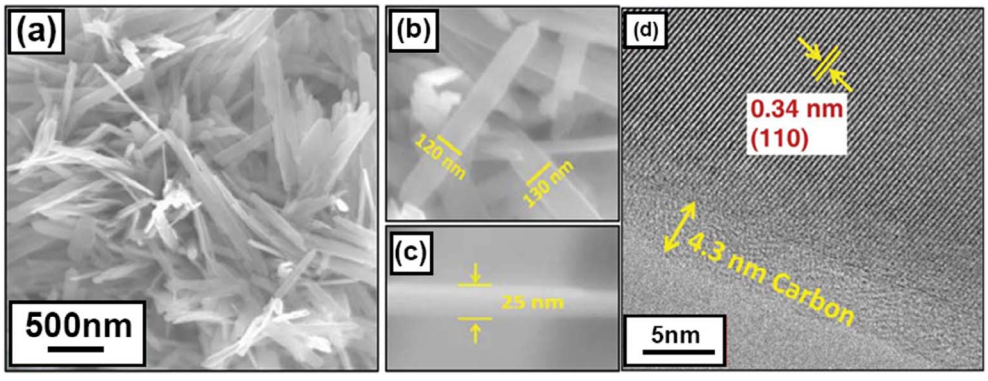

Fig. 21. (a)–(c) SEM images and (d) TEM image of carbon/VO_2 (B) composite with 6.6 wt% carbon content. Adapted from Ref. [148] with permission from The Royal Society of Chemistry.

Table 5
Strategies to improve the thermochromic and electrochemistry properties of VO_2 and the recommended CVD methods for applying the strategies.

Applications	Strategy	Researching direction	Recommended CVD method	Purpose
To improve thermochromic performance	Doping	New element Co-doping	APCVD	• To reduce τ_c, enhance ΔT_{sol} and T_{lum} in thermochromic materials
	Composite formation	Nanocomposite	AACVD, Hybrid AA/APCVD	
		Mixed phase materials	AACVD	• Add multifunction such as photocatalytic to thermochromic materials
		Multi-layered materials	APCVD, MOCVD, ALD	• Add multifunction such as hydrophobicity, photocatalytic and anti-oxidation ability to thermochromic film • Enhance ΔT_{sol} and T_{lum} at the same time
	Template-assisted growth	Biomimetic structure and photonic crystal	APCVD, MOCVD, ALD	• Enhance both T_{lum} and ΔT_{sol} and change colour and optical responses in thermochromic materials
To improve electrochemical performance	Composite formation	Ultra-thin carbon overcoating (~5nm)	ALD	• Enhance conductivity and lithium ion diffusivity to achieve maximum battery performance
		Graphene quantum dot coated VO_2 arrays	ALD, APCVD	• Enhance conductivity, ion diffusivity and durability to achieve maximum battery performance • Capable for both Li-ion and Na-ion battery
		VO_2(B) coated carbon fiber cloth	APCVD, MOCVD	• Balance conductivity, ion diffusivity and durability to achieve maximum battery performance • Potential candidate for flexible Li-ion battery
		VO_x overcoated CNT structure VO_2 nano-sphere decorated CNT	ALD, APCVD	Balance conductivity, specific capacity and cycling durability to maximize supercapacitor performance
	Template-assisted growth	Core-shell structure	APCVD, MOCVD, ALD	• Enhance field emission properties
	Morphology controlling	Controlling crystalline grain size (from ~ 300 nm to ~ 100 nm)	APCVD, MOCVD	• Enhance discharge density and durability
		Highly porous surface morphologies with extremely small surface features (~5 nm)	AACVD	• Enhance electrode/electrolyte interactions and improve cycling performance

and supercapacitor devices. In future studies, the electrochemical properties of VO_2 films can be enhanced with other metal oxides such as Co_3O_4 and TiO_2. Also, it is necessary to study and improve the electrochemical performance of VO_2 thick films, which are much needed for practical energy storage devices. Because of the abundant availability and low price of sodium (Na) and magnesium (Mg), Na-ion and Mg-ion batteries are currently attracting research attention. The applications of VO_2 in Na-ion and Mg-ion batteries would be an interesting topic for future research. Finally, the mass production of VO_2 based batteries and supercapacitors should be discussed in order to translate the VO_2 based product from the laboratory into our daily life.

Lastly, the current discussion of VO_2's application in energy conservation and storage field is still mainly limited to material perspective and aims at the performance improvement of material. The discussion of VO_2 based device in energy perspective is relatively lacking. We suggest that more research can be conducted to focus on the actual impact of VO_2 on energy field such as the amount of energy saving in different region of the world; the optimised design of VO_2 coated smart window (for example the window size, installing location and window-to-wall ratio) for the best building energy saving effect; the contribution of VO_2 based energy storage device to the cost-cutting of electric vehicles; and the stability of the power grid after the introducing of VO_2 based battery or supercapacitor. The discussion based on the energy perspective will not only serve as a guideline for the material research to meet the real-world demand but also accelerate the applying of VO_2 based device in the actual applications.

Acknowledgements

This research is supported by grants from the National Research Foundation, Prime Minister's Office, Singapore under its Campus of Research Excellence and Technological Enterprise (CREATE) programme, Ministry of Education (MOE) Tier one, RG124/16 and NRF2015NRF-POC002-019.

References

[1] Omer AM. Energy, environment and sustainable development. Renew Sustain Energy Rev 2008;12:2265–300.
[2] Omer AM. Energy use and environmental impacts: a general review. J Renew Sustain Energy 2009;1:053101.
[3] Lemmet S. Buildings and climate change: summary for decision-makers Sustainable Buildings & Climate Initiative. Paris: United Nations Environmental Programme; 2009. p. 1–62.
[4] Yang L, Yan H, Lam JC. Thermal comfort and building energy consumption implications – a review. Appl Energy 2014;115:164–73.
[5] Kamalisarvestani M, Saidur R, Mekhilef S, Javadi FS. Performance, materials and coating technologies of thermochromic thin films on smart windows. Renew Sustain Energy Rev 2013;26:353–64.
[6] Cheung CK, Fuller RJ, Luther MB. Energy-efficient envelope design for high-rise apartments. Energy Build 2005;37:37–48.
[7] Synnefa A, Santamouris M, Akbari H. Estimating the effect of using cool coatings on energy loads and thermal comfort in residential buildings in various climatic conditions. Energy Build 2007;39:1167–74.
[8] Baetens R, Jelle BP, Gustavsen A. Properties, requirements and possibilities of smart windows for dynamic daylight and solar energy control in buildings: a state-of-the-art review. Sol Energy Mater Sol Cells 2010;94:87–105.
[9] Tarantini M, Loprieno AD, Porta PL. A life cycle approach to Green Public Procurement of building materials and elements: a case study on windows. Energy 2011;36:2473–82.
[10] Cocker TL, Titova LV, Fourmaux S, Holloway G, Bandulet HC, Brassard D, et al. Phase diagram of the ultrafast photoinduced insulator-metal transition in vanadium dioxide. Phys Rev B 2012;85:155120.
[11] Saeli M, Piccirillo C, Parkin IP, Binions R, Ridley I. Energy modelling studies of thermochromic glazing. Energy Build 2010;42:1666–73.
[12] Li S-Y, Niklasson GA, Granqvist CG. Thermochromic fenestration with VO_2-based materials: three challenges and how they can be met. Thin Solid Films 2012;520:3823–8.
[13] Liu C, Cao X, Kamyshny A, Law JY, Magdassi S, Long Y. VO_2/Si–Al gel nanocomposite thermochromic smart foils: largely enhanced luminous transmittance and solar modulation. J Colloid Interface Sci 2014;427:49–53.
[14] Li S-Y, Niklasson GA, Granqvist CG. Nanothermochromics with VO_2-based core-shell structures: calculated luminous and solar optical properties. J Appl Phys 2011;109:113515.
[15] Gao Y, Wang S, Kang L, Chen Z, Du J, Liu X, et al. VO_2-Sb:SnO_2 composite thermochromic smart glass foil. Energy Environ Sci 2012;5:8234–7.
[16] Kang L, Gao Y, Luo H, Chen Z, Du J, Zhang Z. Nanoporous thermochromic VO_2 films with low optical constants, enhanced luminous transmittance and thermochromic properties. ACS Appl Mater Interfaces 2011;3:135–8.
[17] Qian X, Wang N, Li Y, Zhang J, Xu Z, Long Y. Bioinspired multifunctional vanadium dioxide: improved thermochromism and hydrophobicity. Langmuir 2014;30:10766–71.
[18] Liu C, Wang N, Long Y. Multifunctional overcoats on vanadium dioxide thermochromic thin films with enhanced luminous transmission and solar modulation, hydrophobicity and anti-oxidation. Appl Surf Sci 2013;283:222–6.
[19] Liu C, Balin I, Magdassi S, Abdulhalim I, Long Y. Vanadium dioxide nanogrid films for high transparency smart architectural window applications. Opt Exp 2015;23:A124–32.
[20] Liu C, Long Y, Magdassi S, Mandler D. Ionic strength induced electrodeposition: a universal approach for nanomaterial deposition at selective areas. Nanoscale 2017;9:485–90.
[21] Lu Q, Liu C, Wang N, Magdassi S, Mandler D, Long Y. Periodic micro-patterned VO_2 thermochromic films by mesh printing. J Mater Chem C 2016;4:8385–91.
[22] Zhou Y, Cai Y, Hu X, Long Y. Temperature-responsive hydrogel with ultra-large solar modulation and high luminous transmission for "smart window" applications. J Mater Chem A 2014;2:13550–5.
[23] Zhou Y, Cai Y, Hu X, Long Y. VO_2/hydrogel hybrid nanothermochromic material with ultra-high solar modulation and luminous transmission. J Mater Chem A 2015;3:1121–6.
[24] Zhou Y, Layani M, Boey YCF, Sokolov I, Magdassi S, Long Y. Electro-thermochromic devices composed of self-assembled transparent electrodes and hydrogels. Adv Mater Technol 2016;1:1600069.
[25] Kumar S, Lenoble D, Maury F, Bahlawane N. Synthesis of vanadium oxide films with controlled morphologies: Impact on the metal–insulator transition behaviour. Phys Stat Solidi A 2015;212:1582–7.
[26] Sahana MB, Dharmaprakash MS, Shivashankar SA. Microstructure and properties of VO_2 thin films deposited by MOCVD from vanadyl acetylacetonate. J Mater Chem 2002;12:333–8.
[27] Kang Y-B. Critical evaluation and thermodynamic optimization of the VO–$VO_{2.5}$ system. J Eur Ceram Soc 2012;32:3187–98.
[28] Bahlawane N, Lenoble D. Vanadium oxide compounds: structure, properties, and growth from the gas phase. Chem Vap Depos 2014;20:299–311.
[29] Yan Y, Li B, Guo W, Pang H, Xue H. Vanadium based materials as electrode materials for high performance supercapacitors. J Power Sources 2016;329:148–69.
[30] Dunn B, Kamath H, Tarascon J-M. Electrical energy storage for the grid: a battery of choices. Science 2011;334:928–35.
[31] Miller JR, Simon P. Electrochemical capacitors for energy management. Science 2008;321:651–2.
[32] Simon P, Gogotsi Y, Dunn B. Where do batteries end and supercapacitors begin? Science 2014;343:1210–1.
[33] Köhler J, Makihara H, Uegaito H, Inoue H, Toki M. LiV_3O_8: characterization as anode material for an aqueous rechargeable Li-ion battery system. Electrochim Acta 2000;46:59–65.
[34] Murphy DW, Christian PA, DiSalvo FJ, Carides JN, Waszczak JV. Lithium incorporation by V6O13 and related vanadium (+4, +5) oxide cathode materials. J Electrochem Soc 1981;128:2053–60.
[35] Tsang C, Manthiram A. Synthesis of nanocrystalline VO2 and its electrochemical behavior in lithium batteries. J Electrochem Soc 1997;144:520–4.
[36] Wu C, Xie Y. Promising vanadium oxide and hydroxide nanostructures: from energy storage to energy saving. Energy Environ Sci 2010;3:1191–206.
[37] Huynh WU, Dittmer JJ, Alivisatos AP. Hybrid nanorod-polymer solar cells. Science 2002;295:2425–7.
[38] Subba Reddy CV, Walker Jr EH, Wicker Sr SA, Williams QL, Kalluru RR. Synthesis of VO_2 (B) nanorods for Li battery application. Curr Appl Phys 2009;9:1195–8.
[39] Armstrong G, Canales J, Armstrong AR, Bruce PG. The synthesis and lithium intercalation electrochemistry of VO_2(B) ultra-thin nanowires. J Power Sources 2008;178:723–8.
[40] Liu J, Li Q, Wang T, Yu D, Li Y. Metastable vanadium dioxide nanobelts: hydrothermal synthesis, electrical transport, and magnetic properties. Angew Chem 2004;116:5158–62.
[41] Kannan AM, Manthiram A. Synthesis and electrochemical evaluation of high capacity nanostructured VO_2 cathodes. Solid State Ion 2003;159:265–71.
[42] Liu H, Wang Y, Wang K, Hosono E, Zhou H. Design and synthesis of a novel nanothorn VO_2(B) hollow microsphere and their application in lithium-ion batteries. J Mater Chem 2009;19:2835–40.
[43] Zhang S, Li Y, Wu C, Zheng F, Xie Y. Novel flowerlike metastable vanadium dioxide (B) micronanostructures: facile synthesis and application in aqueous lithium ion batteries. J Phys Chem C 2009;113:15058–67.
[44] Jiang W, Ni J, Yu K, Zhu Z. Hydrothermal synthesis and electrochemical characterization of VO_2 (B) with controlled crystal structures. Appl Surf Sci 2011;257:3253–8.
[45] Luo JY, Xia YY. Aqueous lithium-ion battery $LiTi_2(PO_4)_3$/$LiMn_2O_4$ with high power and energy densities as well as superior cycling stability. Adv Funct Mater 2007;17:3877–84.
[46] Luo S, Tang Z, Lu J, Zhang Z. Electrochemical properties of carbon-mixed $LiFePO_4$ cathode material synthesized by the ceramic granulation method. Ceram Int 2008;34:1349–51.
[47] Wang F, Liu Y, Liu C-y. Hydrothermal synthesis of carbon/vanadium dioxide core–shell microspheres with good cycling performance in both organic and aqueous electrolytes. Electrochim Acta 2010;55:2662–6.

[48] Sun J, Chen Y, Priydarshi MK, Chen Z, Bachmatiuk A, Zou Z, et al. Direct chemical vapor deposition-derived graphene glasses targeting wide ranged applications. Nano Lett 2015;15:5846–54.
[49] Wang N, Huang Y, Magdassi S, Mandler D, Liu H, Long Y. Formation of VO_2 zero-dimensional/nanoporous layers with large supercooling effects and enhanced thermochromic properties. RSC Adv 2013;3:7124–8.
[50] Yue F, Huang W, Shi Q, Li D, Hu Y, Xiao Y, et al. Phase transition properties of vanadium oxide films deposited by polymer-assisted deposition. J Sol-Gel Sci Technol 2014;72:565–70.
[51] Du J, Gao Y, Luo H, Zhang Z, Kang L, Chen Z. Formation and metal-to-insulator transition properties of VO_2–ZrV_2O_7 composite films by polymer-assisted deposition. Sol Energy Mater Sol Cells 2011;95:1604–9.
[52] Wang N, Duchamp M, Xue C, Dunin-Borkowski RE, Liu G, Long Y. Single-crystalline W-doped VO_2 nanobeams with highly reversible electrical and plasmonic responses near room temperature. Adv Mater Interf 2016;3:1600164.
[53] Zhou J, Gao Y, Liu X, Chen Z, Dai L, Cao C, et al. Mg-doped VO_2 nanoparticles: hydrothermal synthesis, enhanced visible transmittance and decreased metal-insulator transition temperature. Phys Chem Chem Phys 2013;15:7505–11.
[54] Mjejri I, Etteyeb N, Sediri F. Mesoporous vanadium oxide nanostructures: hydrothermal synthesis, optical and electrochemical properties. Ceram Int 2014;40:1387–97.
[55] Ke Y, Balin I, Wang N, Lu Q, Tok LYA, White TJ, et al. Two-dimensional SiO_2/VO_2 photonic crystals with statically visible and dynamically infrared modulated for smart window deployment. ACS Appl Mater Interfaces 2016;8:33112–20.
[56] Zhang H-T, Zhang L, Mukherjee D, Zheng Y-X, Haislmaier RC, Alem N, et al. Wafer-scale growth of VO_2 thin films using a combinatorial approach. Nat Commun 2015;6:8475.
[57] Cao X, Thet MN, Zhang Y, Loo SCJ, Magdassi S, Yan Q, et al. Solution-based fabrication of VO_2 (M) nanoparticles via lyophilisation. RSC Adv 2015;5:25669–75.
[58] Lakes RS, Lee T, Bersie A, Wang YC. Extreme damping in composite materials with negative-stiffness inclusions. Nature 2001;410:565–7.
[59] Kim J, Ko C, Frenzel A, Ramanathan S, Hoffman JE. Nanoscale imaging and control of resistance switching in VO_2 at room temperature. Appl Phys Lett 2010;96:213106.
[60] Leroux C, Nihoul G, Van Tendeloo G. From VO_2(B) to VO_2(R): theoretical structures of VO_2 polymorphs and in situ electron microscopy. Phys Rev B 1998;57:5111–21.
[61] Warwick MEA, Binions R. Chemical vapour deposition of thermochromic vanadium dioxide thin films for energy efficient glazing. J Solid State Chem 2014;214:53–66.
[62] Jones AC, Hitchman ML. Chemical vapour deposition. [electronic resource] : precursors, processes and applications. Cambridge, UK: Royal Society of Chemistry; 2009.
[63] Dobkin DM, Zuraw MK. Principles of chemical vapor deposition. [electronic resource]. Dordrecht: Springer Netherlands; 2003.
[64] MacChesney JB, Potter JF, Guggenheim HJ. Preparation and properties of vanadium dioxide films. J Electrochem Soc 1968;115:52–5.
[65] Vernardou D, Pemble ME, Sheel DW. The growth of thermochromic VO_2 films on glass by atmospheric-pressure CVD: a comparative study of precursors, CVD methodology, and substrates. Chem Vap Depos 2006;12:263–74.
[66] Vernardou D, Paterakis P, Drosos H, Spanakis E, Povey IM, Pemble ME, et al. A study of the electrochemical performance of vanadium oxide thin films grown by atmospheric pressure chemical vapour deposition. Sol Energy Mater Sol Cells 2011;95:2842–7.
[67] Gaskell JM, Afzaal M, Sheel DW, Yates HM, Delfanazari K, Muskens OL. Optimised atmospheric pressure CVD of monoclinic VO_2 thin films with picosecond phase transition. Surf Coat Technol 2016;287:160–5.
[68] Manning TD, Parkin IP, Clark RJH, Sheel D, Pemble ME, Vernadou D. Intelligent window coatings: atmospheric pressure chemical vapour deposition of vanadium oxides. J Mater Chem 2002;12:2936–9.
[69] Wilkinson M, Kafizas A, Bawaked SM, Obaid AY, Al-Thabaiti SA, Basahel SN, et al. Combinatorial atmospheric pressure chemical vapor deposition of graded TiO_2–VO_2 mixed-phase composites and their dual functional property as self-cleaning and photochromic window coatings. ACS Comb Sci 2013;15:309–19.
[70] Manning TD, Parkin IP, Pemble ME, Sheel D, Vernardou D. Intelligent window coatings: atmospheric pressure chemical vapor deposition of tungsten-doped vnadium dioxide. Chem Mater 2004;16:744–9.
[71] Manning TD, Parkin IP. Vanadium(IV) oxide thin films on glass and silicon from the atmospheric pressure chemical vapour deposition reaction of $VOCl_3$ and water. Polyhedron 2004;23:3087–95.
[72] Kritikos L, Zambelis L, Papadimitropoulos G, Davazoglou D. Structure and electrical properties of selectively chemically vapor deposited vanadium oxide films from vanadium tri-i-propoxy oxide vapors. Surf Coat Technol 2007;201:9334–9.
[73] Louloudakis D, Vernardou D, Spanakis E, Katsarakis N, Koudoumas E. Thermochromic vanadium oxide coatings grown by APCVD at low temperatures. Phys Proc 2013;46:137–41.
[74] Papadimitropoulos G, Kostis I, Trantalidis S, Tsiatouras A, Vasilopoulou M, Davazoglou D. Investigation of structural, morphological and electrical properties of APCVD vanadium oxide thin films. Phys Stat Solidi C 2015;12:964–8.
[75] Vernardou D, Louloudakis D, Spanakis E, Katsarakis N, Koudoumas E. Thermochromic amorphous VO_2 coatings grown by APCVD using a single-precursor. Sol Energy Mater Sol Cells 2014;128:36–40.
[76] Maruyama T, Ikuta Y. Vanadium dioxide thin films prepared by chemical vapour deposition from vanadium(III) acetylacetonate. J Mater Sci 1993;28:5073–8.
[77] Spanò SF, Toro RG, Condorelli GG, Messina GML, Marletta G, Malandrino G. Phase-selective route to V-O film formation: a systematic MOCVD study into the effects of deposition temperature on structure and morphology. Chem Vap Depos 2015;21:319–26.
[78] Barreca D, Depero LE, Franzato E, Rizzi GA, Sangaletti L, Tondello E, et al. Vanadyl precursors psed to modify the properties of vanadium oxide thin flms obtained by chemical vapor deposition. J Electrochem Soc 1999;146:551–8.
[79] Vernardou D, Pemble ME, Sheel DW. Vanadium oxides prepared by liquid injection MOCVD using vanadyl acetylacetonate. Surf Coat Technol 2004;188–189:250–4.
[80] Barreca D, Armelao L, Caccavale F, Di Noto V, Gregori A, Rizzi GA, et al. Highly oriented V_2O_5 nanocrystalline thin films by plasma-enhanced chemical vapor deposition. Chem Mater 2000;12:98–103.
[81] Kuypers AD, Spee CIMA, Linden JL, Kirchner G, Forsyth JF, Mackor A. Plasma-enhanced CVD of electrochromic materials. Surf Coat Technol 1995;74:1033–7.
[82] Musschoot J, Deduytsche D, Poelman H, Haemers J, Van Meirhaeghe RL, Van den Berghe S, et al. Comparison of thermal and plasma-enhanced ALD/CVD of vanadium pentoxide. J Electrochem Soc 2009;156:122–6.
[83] Zhang JG, Liu P, Turner JA, Tracy CE, Benson DK. Highly stable vanadium oxide cathodes prepared by plasma-enhanced chemical vapor deposition. J Electrochem Soc 1998;145:1889–92.
[84] Marchand P, Hassan IA, Parkin IP, Carmalt CJ. Aerosol-assisted delivery of precursors for chemical vapour deposition: expanding the scope of CVD for materials fabrication. Dalton Trans 2013;42:9406–22.
[85] Naik AJT, Bowman C, Panjwani N, Warwick MEA, Binions R. Electric field assisted aerosol assisted chemical vapour deposition of nanostructured metal oxide thin films. Thin Solid Films 2013;544:452–6.
[86] Piccirillo C, Binions R, Parkin IP. Synthesis and functional properties of vanadium oxides: V_2O_3, VO_2, and V_2O_5 deposited on glass by aerosol-assisted CVD. Chem Vap Depos 2007;13:145–51.
[87] Crane J, Warwick M, Smith R, Furlan N, Binions R. The application of electric fields to aerosol assisted chemical vapor deposition reactions. J Electrochem Soc 2011;158:D62–7.
[88] Warwick MEA, Binions R. On the effects of electric fields in aerosol assisted chemical vapour deposition reactions of vanadyl acetylacetonate solutions in ethanol. J Nanosci Nanotechnol 2011;11:8126–31.
[89] Warwick MEA, Binions R. Electric field assisted aerosol assisted chemical vapor deposition of nanostructured metal oxide thin films. Surf Coat Technol 2013;230:28–32.
[90] Warwick MEA, Ridley I, Binions R. Electric fields in the chemical vapour deposition growth of vanadium dioxide thin films. J Nanosci Nanotechnol 2011;11:8158–62.
[91] Warwick MEA, Ridley I, Binions R. Thermochromic vanadium dioxide thin films from electric field assisted aerosol assisted chemical vapour deposition. Surf Coat Technol 2013;230:163–7.
[92] Warwick MEA, Ridley I, Binions R. Thermochromic vanadium dioxide thin films prepared by electric field assisted atmospheric pressure chemical vapour deposition for intelligent glazing application and their energy demand reduction properties. Sol Energy Mater Sol Cells 2016;157:686–94.
[93] Warwick MEA, Binions R. Thermochromic vanadium dioxide thin films from electric field assisted aerosol assisted chemical vapour deposition. Sol Energy Mater Sol Cells 2015;143:592–600.
[94] Warwick MEA, Dunnill CW, Goodall J, Darr JA, Binions R. Hybrid chemical vapour and nanoceramic aerosol assisted deposition for multifunctional nanocomposite thin films. Thin Solid Films 2011;519:5942–8.
[95] Blanquart T, Niinisto J, Gavagnin M, Longo V, Heikkila M, Puukilainen E, et al. Atomic layer deposition and characterization of vanadium oxide thin films. RSC Adv 2013;3:1179–85.
[96] Premkumar PA, Martens K, Rampelberg G, Toeller M, Ablett JM, Meersschaut J, et al. Metal-insulator transition in ALD VO_2 ultrathin films and nanoparticles: morphological control. Adv Funct Mater 2015;25:679–86.
[97] Premkumar PA, Toeller M, Radu IP, Adelmann C, Schaekers M, Meersschaut J, et al. Process study and characterization of VO_2 thin films synthesized by ALD using TEMAV and O_3 precursors. ECS J Solid State Sci Technol 2012;1:P169–74.
[98] Tangirala M, Zhang K, Nminibapiel D, Pallem V, Dussarrat C, Cao W, et al. Physical analysis of VO_2 films grown by atomic layer deposition and RF magnetron sputtering. ECS J Solid State Sci Technol 2014;3:N89–94.
[99] Rampelberg G, Schaekers M, Martens K, Xie Q, Deduytsche D, Schutter BD, et al. Semiconductor-metal transition in thin VO_2 films grown by ozone based atomic layer deposition. Appl Phys Lett 2011;98:162902.
[100] Kim C-Y, Kim SH, Kim SJ, An K-S. VO_2(1 1 0) film formation on TiO_2(1 1 0) through post-reduction of ALD grown vanadium oxide. Appl Surf Sci 2014;313:368–71.
[101] Dagur P, Mane AU, Shivashankar SA. Thin films of VO_2 on glass by atomic layer deposition: microstructure and electrical properties. J Cryst Growth 2005;275:e1223–8.
[102] Chen X, Pomerantseva E, Banerjee P, Gregorczyk K, Ghodssi R, Rubloff G. Ozone-based atomic layer deposition of crystalline V_2O_5 films for high performance electrochemical energy storage. Chem Mater 2012;24:1255–61.
[103] Musschoot J, Deduytsche D, Van Meirhaeghe RL, Detavernier C. ALD of vanadium oxide. ECS Trans 2009;25:29–37.
[104] Suntola T. Atomic layer epitaxy. Mater Sci Rep 1989;4:261–312.
[105] Romanyuk A, Steiner R, Marot L, Oelhafen P. Temperature-induced metal–semiconductor transition in W-doped VO_2 films studied by photoelectron spectroscopy. Sol Energy Mater Sol Cells 2007;91:1831–5.
[106] Blackman CS, Piccirillo C, Binions R, Parkin IP. Atmospheric pressure chemical vapour deposition of thermochromic tungsten doped vanadium dioxide thin films

for use in architectural glazing. Thin Solid Films 2009;517:4565–70.
[107] Manning TD, Parkin IP. Atmospheric pressure chemical vapour deposition of tungsten doped vanadium(iv) oxide from $VOCl_3$, water and WCl_6. J Mater Chem 2004;14:2554–9.
[108] Binions R, Hyett G, Piccirillo C, Parkin IP. Doped and un-doped vanadium dioxide thin films prepared by atmospheric pressure chemical vapour deposition from vanadyl acetylacetonate and tungsten hexachloride: the effects of thickness and crystallographic orientation on thermochromic properties. J Mater Chem 2007;17:4652–60.
[109] Binions R, Piccirillo C, Palgrave RG, Parkin IP. Hybrid aerosol assisted and atmospheric pressure CVD of gold-doped vanadium dioxide. Chem Vap Depos 2008;14:33–9.
[110] Vernardou D, Pemble ME, Sheel DW. Tungsten-doped vanadium oxides prepared by direct liquid injection MOCVD. Chem Vap Depos 2007;13:158–62.
[111] Piccirillo C, Binions R, Parkin IP. Nb-doped VO_2 thin films prepared by aerosol-assisted chemical vapour deposition. Eur J Inorg Chem 2007;2007:4050–5.
[112] Burkhardt W, Christmann T, Meyer BK, Niessner W, Schalch D, Scharmann A. W- and F-doped VO_2 films studied by photoelectron spectrometry. Thin Solid Films 1999;345:229–35.
[113] Kiri P, Warwick MEA, Ridley I, Binions R. Fluorine doped vanadium dioxide thin films for smart windows. Thin Solid Films 2011;520:1363–6.
[114] Manning TD, Parkin IP, Blackman C, Qureshi U. APCVD of thermochromic vanadium dioxide thin films-solid solutions V2-xMxO2 (M = Mo, Nb) or composites VO2: SnO2. J Mater Chem 2005;15:4560–6.
[115] Burkhardt W, Christmann T, Franke S, Kriegseis W, Meister D, Meyer BK, et al. Tungsten and fluorine co-doping of VO_2 films. Thin Solid Films 2002;402:226–31.
[116] Binions R, Piccirillo C, Parkin IP. Tungsten doped vanadium dioxide thin films prepared by atmospheric pressure chemical vapour deposition from vanadyl acetylacetonate and tungsten hexachloride. Surf Coat Technol 2007;201:9369–72.
[117] Chen S, Dai L, Liu J, Gao Y, Liu X, Chen Z, et al. The visible transmittance and solar modulation ability of VO_2 flexible foils simultaneously improved by Ti doping: an optimization and first principle study. Phys Chem Chem Phys 2013;15:17537–43.
[118] Du J, Gao Y, Luo H, Kang L, Zhang Z, Chen Z, et al. Significant changes in phase-transition hysteresis for Ti-doped VO_2 films prepared by polymer-assisted deposition. Sol Energy Mater Sol Cells 2011;95:469–75.
[119] Wang N, Liu S, Zeng XT, Magdassi S, Long Y. Mg/W-codoped vanadium dioxide thin films with enhanced visible transmittance and low phase transition temperature. J Mater Chem C 2015;3:6771–7.
[120] Batista C, Ribeiro RM, Teixeira V. Synthesis and characterization of VO_2-based thermochromic thin films for energy-efficient windows. Nanoscale Res Lett 2011;6:301.
[121] Greenberg CB. Undoped and doped VO_2 films grown from $VO(OC_3H_7)_3$. Thin Solid Films 1983;110:73–82.
[122] Béteille F, Livage J. Optical switching in VO_2 thin films. J Sol-Gel Sci Technol 1998;13:915–21.
[123] Lee M-H, Kim M-G, Song H-K. Thermochromism of rapid thermal annealed VO_2 and Sn-doped VO_2 thin films. Thin Solid Films 1996;290–291:30–3.
[124] Chen B, Yang D, Charpentier PA, Zeman M. Al^{3+}-doped vanadium dioxide thin films deposited by PLD. Sol Energy Mater Sol Cells 2009;93:1550–4.
[125] Phillips TE, Murphy RA, Poehler TO. Electrical studies of reactively sputtered Fe-doped VO_2 thin films. Mater Res Bull 1987;22:1113–23.
[126] Song L, Zhang Y, Huang W, Shi Q, Li D, Zhang Y, et al. Preparation and thermochromic properties of Ce-doped VO_2 films. Mater Res Bull 2013;48:2268–71.
[127] Ufert KD. Doping of VO_2 thin films by ion implantation. Phys Status Solidi A 1977;42:187–90.
[128] Gao Y, Cao C, Dai L, Luo H, Kanehira M, Ding Y, et al. Phase and shape controlled VO_2 nanostructures by antimony doping. Energy Environ Sci 2012;5:8708–15.
[129] Wang N, Duchamp M, Dunin-Borkowski RE, Liu S, Zeng X, Cao X, et al. Terbium-doped VO_2 thin films: reduced phase transition temperature and largely enhanced luminous transmittance. Langmuir 2016;32:759–64.
[130] Wang N, Chew Shun NT, Duchamp M, Dunin-Borkowski RE, Li Z, Long Y. Effect of lanthanum doping on modulating the thermochromic properties of VO_2 thin films. RSC Adv 2016;6:48455–61.
[131] Cao X, Wang N, Magdassi S, Mandler D, Long Y. Europium doped vanadium dioxide material: reduced phase transition temperature, enhanced luminous transmittance and solar modulation. Sci Adv Mater 2014;6:558–61.
[132] Mlyuka NR, Niklasson GA, Granqvist CG. Mg doping of thermochromic VO_2 films enhances the optical transmittance and decreases the metal-insulator transition temperature. Appl Phys Lett 2009;95:171909.
[133] Li S-Y, Niklasson GA, Granqvist CG. Nanothermochromics: calculations for VO_2 nanoparticles in dielectric hosts show much improved luminous transmittance and solar energy transmittance modulation. J Appl Phys 2010;108:063525.
[134] Li S-Y, Mlyuka NR, Primetzhofer D, Hallén A, Possnert G, Niklasson GA, et al. Bandgap widening in thermochromic Mg-doped VO_2 thin films: quantitative data based on optical absorption. Appl Phys Lett 2013;103:161907.
[135] Shen N, Chen S, Chen Z, Liu X, Cao C, Dong B, et al. The synthesis and performance of Zr-doped and W-Zr-codoped VO_2 nanoparticles and derived flexible foils. J Mater Chem A 2014;2:15087–93.
[136] Wang N, Goh QS, Lee PL, Magdassi S, Long Y. One-step hydrothermal synthesis of rare earth/W-codoped VO_2 nanoparticles: Reduced phase transition temperature and improved thermochromic properties. J Alloys Compd 2017;711:222–8.
[137] Saeli M, Piccirillo C, Parkin IP, Ridley I, Binions R. Nano-composite thermochromic thin films and their application in energy-efficient glazing. Sol Energy Mater Sol Cells 2010;94:141–51.
[138] Saeli M, Binions R, Piccirillo C, Hyett G, Parkin IP. Templated growth of smart nanocomposite thin films: hybrid aerosol assisted and atmospheric pressure chemical vapour deposition of vanadyl acetylacetonate, auric acid and tetraoctyl ammonium bromide. Polyhedron 2009;28:2233–9.
[139] Qureshi U, Manning TD, Parkin IP. Atmospheric pressure chemical vapour deposition of VO_2 and VO_2/TiO_2 films from the reaction of $VOCl_3$, $TiCl_4$ and water. J Mater Chem 2004;14:1190–4.
[140] Qureshi U, Manning TD, Blackman C, Parkin IP. Composite thermochromic thin films: (TiO_2)–(VO_2) prepared from titanium isopropoxide, $VOCl_3$ and water. Polyhedron 2006;25:334–8.
[141] Evans P, Pemble ME, Sheel DW, Yates HM. Multi-functional self-cleaning thermochromic films by atmospheric pressure chemical vapour deposition. J Photochem Photobiol, A 2007;189:387–97.
[142] Breckenfeld E, Kim H, Burgess K, Charipar N, Cheng SF, Stroud R, et al. Strain effects in epitaxial VO_2 thin films on columnar buffer-layer TiO_2/Al_2O_3 virtual substrates. ACS Appl Mater Interfaces 2017;9:1577–84.
[143] Taylor A, Parkin I, Noor N, Tummeltshammer C, Brown MS, Papakonstantinou I. A bioinspired solution for spectrally selective thermochromic VO_2 coated intelligent glazing. Opt Exp 2013;21:A750–64.
[144] Ke Y, Wen X, Zhao D, Che R, Xiong Q, Long Y. Controllable fabrication of two-dimensional patterned VO_2 nanoparticle, nanodome, and nanonet arrays with tunable temperature-dependent localized surface plasmon resonance. ACS Nano 2017.
[145] Yin H, Yu K, Song C, Wang Z, Zhu Z. Low-temperature CVD synthesis of patterned core-shell VO_2@ZnO nanotetrapods and enhanced temperature-dependent field-emission properties. Nanoscale 2014;6:11820–7.
[146] Vernardou D, Apostolopoulou M, Louloudakis D, Katsarakis N, Koudoumas E. Electrochemical performance of vanadium oxide coatings grown using atmospheric pressure CVD. Chem Vap Depos 2015;21:369–74.
[147] Warwick MEA, Roberts AJ, Slade RCT, Binions R. Electric field assisted chemical vapour deposition - a new method for the preparation of highly porous supercapacitor electrodes. J Mater Chem A 2014;2:6115–20.
[148] Rui X, Sim D, Xu C, Liu W, Tan H, Wong K, et al. One-pot synthesis of carbon-coated VO_2(B) nanobelts for high-rate lithium storage. RSC Adv 2012;2:1174–80.
[149] Chao D, Zhu C, Xia X, Liu J, Zhang X, Wang J, et al. Graphene quantum dots coated VO_2 arrays for highly durable electrodes for Li and Na ion batteries. Nano Lett 2015;15:565–73.
[150] Li S, Liu G, Liu J, Lu Y, Yang Q, Yang L-Y, et al. Carbon fiber cloth@VO_2 (B): excellent binder-free flexible electrodes with ultrahigh mass-loading. J Mater Chem A 2016;4:6426–32.
[151] Wang H, Yi H, Chen X, Wang X. One-step strategy to three-dimensional graphene/VO_2 nanobelt composite hydrogels for high performance supercapacitors. J Mater Chem A 2014;2:1165–73.
[152] Boukhalfa S, Evanoff K, Yushin G. Atomic layer deposition of vanadium oxide on carbon nanotubes for high-power supercapacitor electrodes. Energy Environ Sci 2012;5:6872–9.
[153] Jampani PH, Kadakia K, Hong DH, Epur R, Poston JA, Manivannan A, et al. CVD derived vanadium oxide nano-sphere-carbon nanotube (CNT) nano-composite hetero-structures: high energy supercapacitors. J Electrochem Soc 2013;160:A1118–27.